Joint Centre for Mesoscale Meteorology, Reading, UK

Diagnostic study of a narrow cold frontal rainband and severe winds associated with a stratospheric intrusion

K. A. Browning
R. Reynolds

Internal Report No. 7

August 1993

Met Office Joint Centre for Mesoscale Meteorology Department of Meteorology
University of Reading PO Box 243 Reading RG6 6BB United Kingdom
Tel: +44 (0)118 931 8425 Fax: +44 (0)118 931 8791
www.metoffice.com

Diagnostic study of a narrow cold frontal rainband and severe winds associated with a stratospheric intrusion

K. A. Browning

Joint Centre for Mesoscale Meteorology*
University of Reading
Berks, UK

and

R. Reynolds

Department of Meteorology
University of Reading
Berks, UK

* The Joint Centre for Mesoscale Meteorology is supported by the Meteorological Office and the Department of Meteorology, University of Reading.

Abstract

A diagnostic study is presented of a severe wind event associated with a cold front, using output from an operational numerical weather prediction model together with radar and satellite imagery and detailed surface observations. An intrusion of stratospheric air, initially with a potential vorticity of 2 PV units, is shown to have plunged, as part of a backward-tilted filament, down to the lower troposphere where it was associated with a narrow cold frontal rainband at its leading edge and produced severe wind gusts (up to 70 knots). A close correspondence in time and space is revealed between these surface events and the appearance in the model of a pocket of diluted stratospheric air (with PV=1) at the 2 km level. The stratospheric intrusion produced two distinguishable wind surges: one behind the narrow cold frontal rainband itself and another, which was mainly dry, about 200 km farther behind . The strength of the winds was attributable to the downward transport of momentum as part of the large scale dynamics: local moist processes played only a minor role. At coarse resolution the radar echo from the narrow cold frontal rainband resembled line convection but there are shown to have been significant differences between this event and the archetypal form of line convection often seen in the UK.

1. Introduction

The passage of active cold fronts is often characterized by a narrow band of heavy rain. Houze et al (1976) adopted the term narrow cold frontal rainband (NCFR) to describe such a band. This paper presents a case study of a NCFR and of a stratospheric intrusion that appeared to be causing both it and an area of severe surface winds. The rainband as seen by radar was both narrow and shallow, and was superficially similar to line convection (Browning and Harrold 1970), but its synoptic setting and the accompanying surface winds were significantly different from those associated with line convection as usually observed in the British Isles. Therefore, we shall introduce this study by contrasting its synoptic setting with that of line convection as we are accustomed to observe it.

In the British Isles NCFRs that are intense often occur at those cold fronts that also generate broader bands of light or moderate rain. Using the traditional terminology as applied by Sansom (1951), such fronts are ana cold fronts. The warm conveyor belt associated with such fronts, although orientated predominantly parallel to the front, is characterized by a rearward component of flow relative to the front, leading to a zone of rearward-sloping ascent above the cold frontal zone (Browning 1986). The gentle rearward sloping ascent produces the wide band of light to moderate rain, but embedded within it, at the surface cold front, the ascent may occur more abruptly in the lowest 3 km of the troposphere to give a NCFR with heavy rain. The NCFR in the present study, although also very shallow and producing some moderately heavy rain, occurred in association with what Sansom (1951) would have called a kata cold front: the flow above it had a component forward relative to the front and there was no rearward upslope motion above the front to generate a broad band of rain there.

NCFRs contain fine structure, as described by Hobbs and Biswas (1979) and James and Browning (1979), but those at ana cold fronts are, broadly speaking, organized two-dimensionally: hence the term line convection used by Browning and Harrold (1970). Studies of many ana cold fronts over the British Isles (Browning and Pardoe 1973, James and Browning 1979) have shown that the associated line convection is characterised by a structure

and weather sequence that is remarkably similar from one case to another. The present case differs from line convection in that the strongest winds occurred after rather than before the passage of the NCFR. Moreover, the veer in the wind accompanying the passage of the NCFR occurred more gradually, in association with a rather more segmented rainband structure than is normally encountered with line convection.

The purpose of the present study is to diagnose, with the aid of observational data and model output, the structure and large scale forcing of this particular NCFR and of the severe winds that followed it. We have used a combination of satellite and radar imagery, surface observations and analyses from an operational numerical weather prediction model into which routine observational data are assimilated continuously. The imagery and model output have been manipulated on a versatile workstation system developed at the Joint Centre for Mesoscale Meteorology. The model used is the hydrostatic limited area forecast version of the Meteorological Office Unified Forecast/Climate Model (Cullen 1991). This has a horizontal grid of about 50 km and twenty levels in the vertical. The equations are integrated in spherical polar coordinates (coordinate pole located at 30°N, 160°E) and a hybrid vertical coordinate is used. The global atmospheric version of the Unified Model drives the limited area version by generating values of the prognostic variables in a boundary zone.

2. The NCFR and its synoptic setting

The case to be presented occurred over the British Isles on 23 December 1991 in association with the trailing cold front of a deep low travelling rapidly eastward over Scandinavia. The Central Forecasting Office surface analysis in Fig 1 shows a primary cold front over southern England at 12 UTC, with a short secondary trough some 200 km behind it. Extensive upper cloud accompanied the cold front over the North Sea but over the British Isles the cloud associated with the cold front was shallow (Fig 2).

The UK weather radar network showed a broad region of patchy moderate-to-heavy rain over central northern England and north Wales, and a well defined isolated NCFR at the primary cold front over SE England and the Channel (Fig 3(a)). There was no rain associated with the secondary trough at this time. There was some evidence of a NCFR embedded within the region of extensive rain in northern areas but the present paper focusses on the NCFR that developed farther south where the stronger winds occurred. The progression of this part of the NCFR across the radar network area is shown in Fig 3(b). For most of the time the associated precipitation was weak (0-2 mm h^{-1}) but when the NCFR reached SE England (Fig 3(a)) the rainfall intensified, exceeding 8 and even 16 mm h^{-1} in places. The component of motion of the rainband normal to itself was 22 m s^{-1}. Identifiable parts of the rainband travelled very rapidly, at 32 m s^{-1} from 265°. The zoomed Meteosat infra-red picture in Fig 4, with levels set to resolve the NCFR, shows that the associated cloud top temperatures were mainly between 0 and -5°C. According to radiosonde ascents just ahead of the surface cold front, this indicates a maximum cloud top height for the rainband over central southern England of only 2.0 to 2.7 km (800 to 730 mb),

NCFRs viewed by radar at high resolution are generally composed of line elements separated by small gaps, with occasional large gaps which are referred to by James and Browning (1979) as steps. Normally the line elements correspond to regions of sharp frontal transition whilst the gaps, or at least the larger gaps, correspond to more diffuse frontal

transitions. The radar network composite display (Fig 3), with its 5 km resolution, resolved the steps but not the gaps. Fig 5 depicts the higher-resolution (2 km) output from one of the network radars which shows that the line was composed of precipitation cores or line elements typically 3 km wide and 10 to 20 km long. The line elements were oriented at 30 to 40° to the overall line. These characteristics are similar to those reported for the NCFRs near the NW coast of the United States (Hobbs and Biswas 1979). The length of the elements is also rather similar to the mean length reported by James and Browning (1979); however, their line convection elements were orientated at a smaller angle with respect of the overall line (<20°) thereby giving the overall line convection a less segmented appearance than in the case of the present NCFR. We believe that this is a significant distinction. We suspect that, provided the precipitation is neither intense nor extensive, the orientation of the elements is an indication of the overall sharpness of the surface front. When, as in the present case, the elements are orientated at a large angle to the overall line, since the elements tend to travel more nearly along their own length, most places experience the more gradual windshift associated with the passage of the gaps.

3. The surface winds at and behind the NCFR

The distinction between this NCFR and line convection at an ana cold front was very clear at the surface. Normally the pressure kick and temperature fall at the passage of line convection is accompanied by a sharp veer and decrease in the wind (see, for example, Fig 6(b)). On this occasion, as already noted, the wind shift was relatively gradual: for example, a 40 deg veer in 25 minutes for the first wind surge in Fig 6(a) compared with a 90 deg veer within a few minutes in Fig 6(b). Moreover, the strongest winds on this occasion occurred after the passage of the NCFR, ie, there was a wind increase rather than a decrease with the passage of the NCFR.

Fig 7 shows the overall distribution of gusts in excess of 55 knots (28 m s^{-1}) associated with the period of strong winds behind the NCFR. A broad swath of severe wind gusts, up to 500 km wide in the north-south direction, traversed west to east between 07 and 18 UTC. The strong winds began to decrease after the NCFR reached the Netherlands and there were few gusts in excess of 55 knots after 18 UTC.

Fig 8(a) shows station plots representing the weather sequence accompanying the passage of the primary cold front and associated NCFR, together with isochrones of the initiation of the veer associated with it. Comparison with Fig 3(b) confirms this to be the same feature as the NCFR detected by the radar. Most stations except some bordering the Irish Sea experienced a burst of moderate rain but the speed and narrowness of the NCFR meant that rainfall accumulations were slight. Except over Ireland, all stations experienced a small drop in temperature and relative humidity, as well as a small rise (~ 1 mb) in pressure. The wind veer of between 15 and 50 deg occurred over tens of minutes. In some places the veer occurred in rather less than 20 min but even there it did not occur abruptly as in the example shown in Fig 6(b). Maximum gusts were mainly in the range 50 to 70 knots although rather less during the early stages when the front was crossing Ireland. The peak gust occurred within 30 min of the brief (5 - 15 min) burst of rain marking the NCFR: out of 17 stations with good quality records, it was found that in 3 places the peak gust occurred within 10 min (14 km) of the midpoint of the rainband, in 5 places it occurred more than 20 min after (28 km), but in the majority (9) it occurred between 10 and 20 min after.

A second wind surge, associated with the secondary trough analyzed by CFO (Fig 1), occurred some 200 km behind the NCFR. It was not quite as coherent as the first wind surge and, over the Irish Sea, it appeared to split into two portions propagating at different velocities. Yet another wind surge was identified over central England and eastern England between these two surges but for simplicity we shall concentrate on the two main ones. Fig 8(b) shows isochrones of the initiation of the wind veer associated with the second main wind surge, together with station plots. Except over Ireland this second wind surge was accompanied by little if any rain and relatively small changes in temperature and relative humidity. The maximum gusts were typically 40 knots over central and eastern England (see, eg, Fig 6(a)) but were as high as 60 to 70 knots over Ireland, west Wales and the Netherlands coast.

The chief difference between the two main surges is that the first one followed a brief burst of moderate to heavy rain whereas the second one was dry in most places. Both surges produced severe gusts, however, indicating that, at least in the case of the second surge, the strength of the winds was due to something other than moist processes alone. We show later that the strong wind gusts and the NCFR were associated with a major intrusion of stratospheric air characterized by high potential vorticity and low relative humidity. We suggest the possibility that different portions of the same intrusion were forcing both the wet primary cold front and the dry secondary trough. Koch and Kocin (1991) have observed a similar relationship between a NCFR with strong winds and a stratospheric intrusion in the eastern United States.

4. Structure of the cold frontal region with which the NCFR was associated

Fig 9 depicts the structure of the frontal region, as derived from the Unified Model, within a cross-section through SE England normal to the NCFR. The abscissa gives the distance from the primary surface cold front as determined from the radar-observed NCFR (represented in Fig 9(a) by the vertical arrow up to 730 mb). The correspondence between the observed NCFR and the model output is good. In particular, the NCFR was located in a virtually saturated region of ascent (Fig 9(a)) associated with the cyclonically sheared layer of neutral static stability (ie. θ_w constant with height) just in advance of the leading edge of air with lower θ_w (Fig 9(b)). This is similar to what one would have expected for line convection at an ana cold front (Browning 1986); the main factor in Fig 9(a) that distinguishes this as a kata rather than ana frontal case is the penetration of dry air from the cold side over the top of the NCFR. A related factor that is consistent with this being a kata cold front is the existence of a component of the wind overtaking the front ($U>0$) at all levels above the line convection (Fig 9(c)). This was associated with a major intrusion of air with high potential vorticity (PV), represented in Fig 9(c) by the closed PV = 2 contour (in units of $10^{-6}\,Km^2\,kg^{-1}s^{-1}$).

5. The intrusion of stratospheric air into the troposphere

An informative way of examining the dynamics of a frontal region is to analyse PV, air motion and relative humidity on an isentropic surface (constant θ) that intersects the frontal zone. We have done this (Fig 10) at a sequence of times (0, 6 and 12 UTC) for the θ=300K surface. Over the region of interest, this surface extended from a height of 6 km on the cold side to 3 km on the warm side. The 300 K surface cuts through the middle of the

major intrusion of high-PV stratospheric air (tropopause fold) that was wrapped around the leading edge of the outbreak of cold air (see vertical section in Fig 11). We now examine Figs 10 and 11 in more detail.

Figs 10(a), (b) and (c) show the PV anomaly within the troposphere travelling rapidly (35 m s^{-1}) from left to right. A value of PV equal to 2 or more corresponds to stratospheric air (Hoskins et al 1985) which in this case was intruding into the troposphere in the form of a 2000 km-long backward-tilted filament that was becoming thinner with time. This process is an example of what Thorncroft et al (1993) called 'equatorward Rossby-wave breaking', and corresponds to their anticyclonic category of upper air trough. The vertical section in Fig 11 is along the axis of this PV filament. At 12 UTC (Figs 10(c) and 11) a portion of the filament, over England and Wales, was in the process of cutting off; we discuss this later, in Sec 6.

Figs 10 (d), (e) and (f) show a large region of dry descent (4 cm s^{-1}) associated with the cold airmass behind the axis of the PV filament. Ahead of the filament was a region of moist air associated with the warm airmass; this was narrowing with time as the cold outbreak encroached upon it.

Figs 10 (g), (h) and (i) show the relative flow on the isentropic surface. The streamlines are only approximate because the system velocity used (35 m s^{-1} to the right of the figure everywhere) was not applicable to all parts of the figure. The main feature to note is the confluence, along the axis of the PV filament, between the descending air behind and air apparently ascending up the isentropic surface ahead of it. In fact the Unified Model showed negligible ascent at this level, perhaps because the isentropic surface was itself descending. (The rearward component of flow ahead of the filament is not at variance with the evidence in Fig 9(c) of forward flow relative to the NCFR. This is because the propagation velocity of the PV filament was far higher than that of the NCFR and so the whole pattern aloft was overtaking the NCFR at the surface cold front).

The catching up of the surface cold front by the region of descending stratospheric air is revealed by vertical cross sections at two times (Figs 12(a) and (b)) taken through the cutting-off portion of the PV filament. Between 0 and 12 UTC the area of maximum descent advanced from a position 850 km behind the surface cold front to 550 km behind. The cold frontal zone, represented by the front-parallel component of velocity, steepened during the same period. The centre of the PV filament advanced from 600 km to within 160 km of the surface cold front. Not only was the stratospheric intrusion catching up with the surface front but so too was the region of severe surface gusts. When the surface front was over the west coast of Wales, at 09 UTC, Fig 7 shows that the main region of severe gusts was over western Ireland. By 15 UTC, as the front reached the continental coast, the region of severe gusts had almost caught up with the front.

6. The plunging of the stratospheric intrusion into the top of the boundary layer and its relationship to severe surface gustiness

As already noted in connection with Figs 10(c) and 11, part of the stratospheric intrusion, manifested by the high-PV filament, became cut-off within the troposphere. This was associated with a pronounced local lowering in the base of the PV filament (see Fig 13).

Between 0 and 12 UTC the extent of the PV=2 surface shrank at the 3.5 km level (Fig 13(a)) but air with PV=2 extended down to 3.0 km during the same period. Fig 13(b) suggests that the extension down to 3 km occurred early in the period. Further downward extension of stratospheric air is thought to have led to the expanding area of PV=1 at the 2 km level (Fig 13(c)).

The 12 UTC radiosonde ascent for Camborne, 50 km behind the line convection (Fig 14), shows extremely dry air (relative humidity <1%), of probable stratospheric origin, down to below 2.5 km (750 mb). This air was travelling at about 80 knots (40 m s^{-1}) from 270° just above a region of veered and rather lighter winds (though still strong) within the boundary layer. The vector wind change between heights of 1.5 (850 mb) and 2 km (800 mb) was as much as 20 m s^{-1}. Large fluctuations in relative humidity can be seen near the 800 mb level. These fluctuations were probably associated with intense turbulence at the strongly sheared interface between the descending stratospheric air and the boundary layer. The associated mixing of stratospheric air through the inversion capping the boundary layer would account for the model-derived increase in PV at 800 mb. Fig 13(c) shows that the extent of PV=1 (diluted stratospheric air) at 800 mb increased between 9 and 15 UTC as the stratospheric intrusion traversed rapidly (35 m s^{-1}) across the southern parts of the British Isles before decreasing to zero at 18 UTC as the system weakened over the Netherlands.

The stratospheric intrusion was accompanied by fairly dry air all the way from the lower troposphere up to the stratosphere. This deep layer of dry air appears in the Meteosat water vapour imagery (Fig 15) as a dark zone (high brightness temperature) because here the satellite radiometer was sensing radiation emitted mainly from water vapour in the warm lower troposphere. The sequence of water vapour images in Fig 15 shows that the dark zone developed rapidly during the period 6 to 15 UTC during which stratospheric air was extending down into the boundary layer. The series of tracings in Fig 15(e), when compared with Fig 13(c), shows that the centre of the dark zone tracked closely in line with the lowest part of the stratospheric intrusion and about 150 km or 1½ hours ahead of it. This difference is scarcely above the registration noise between the model and imagery products and gives general support to the validity of the model output.

Comparison of Fig 13(c) with Fig 7 shows that the area where stratospheric air is believed to have penetrated down towards the boundary layer corresponds well to the location and extent of severe winds gusting to over 55 knots. The envelope of severe wind gusts in Fig 7 encompasses both major wind surges (at least at 12 UTC and 18 UTC when they both were severe). It is presumed that the two wind surges (ie those analyzed in Figs 8(a) and (b)) corresponded to fine structure in the PV pattern that the model was unable to resolve. The close correspondence between the descending PV maximum and the severe surface gusts is consistent with a causal relationship and it suggests a possible method for forecasting damaging surface winds. The method might be based on model prediction of the appearance of a fast-moving small area of recently-descended air with PV=1 at the 2 km level, say. Support for the model prediction might be obtained by looking for the appearance of a corresponding dark zone in the satellite water vapour imagery.

7. The role of moist processes at the NCFR.

A case has been made in the previous sections for the stratospheric intrusion being responsible for the overall area of severe surface winds behind the NCFR. This was composed of (at least) two major wind surges. The second of these (Fig 8(b)) was accompanied by hardly any rain, except over Ireland, and moist processes are unlikely to have been involved to a significant degree. In the case of the first wind surge the situation was more complicated: for a large proportion of the time its leading edge was defined by the NCFR, and moist processes (eg downdraughts driven by evaporation and melting) might be expected to have played a role in strengthening the surface gusts. However, contingency tables (not shown) derived from the data in Fig 8(b), displayed no clear relationship between the strength of the gusts and either the occurrence or intensity of rain. This suggests that the moist processes were not playing a dominant role in determining the strength of the surface gusts. On the other hand, there is some limited evidence in Fig 8(a) of a relationship over the British Isles between the occurrence of rain and a briefly overshooting wind veer. Of the 18 observations of overshooting only one occurred without rain, whereas in the case of the 27 observations with no overshooting as many as 5 occurred without rain. Furthermore, amongst the 18 cases of overshooting, 14 occurred over the central, eastern and southeastern parts of England between 1130 and 1400 UTC (Fig 8(a)), where radar measurements of the NCFR suggested that rainfall intensities averaged over 5 km were reaching values in excess of 4 mm h^{-1}, with local maxima above 16 mm h^{-1} (see for example Fig 3(a)). This is consistent with the view that moist processes were producing a local enhancement of the wind superimposed upon a pattern of strong winds that was determined mainly by other factors. The location of the NCFR at the leading edge of the region of strong surface winds, and the fact that the NCFR became more intense at about 12 UTC as the stratospheric intrusion caught up with it (Sec. 5), is consistent with a causal relationship between the stratospheric intrusion and the intensifying NCFR. We cannot be sure that the stratospheric intrusion was the main driving force throughout the lifetime of the NCFR but it almost certainly did play a major role during its more intense phase.

Many previous studies have concluded that a density current plays an important part in sustaining the shallow convection responsible for NCFRs. In the NCFR events studied by Carbone (1982), Parsons et al (1987) and Koch and Kocin (1991), the strongest winds occurred just behind the NCFR. This effectively produced post-frontal winds that were directed towards the NCFR, as is characteristic of density currents. In fact, given the NCFR speed of 22 m s^{-1} and the surface wind gusts of 55 knots (28 m s^{-1}), there is some evidence to suggest that a density current might have existed in the present case, too. However, to qualify as a density current phenomenon, two further criteria must be satisfied (Smith and Reeder 1988): (1) the density current depth predicted hydrostatically from the surface temperature and pressure changes accompanying frontal passage must be comparable with that deduced from nearby radiosonde ascents, and (2) the motion of the NCFR must be consistent with that predicted from density current theory.

As discussed by Smith and Reeder, the first of these criteria is very difficult to apply because the predicted depth of the density current is highly sensitive to uncertainties in estimating the mean layer-averaged change in temperature. The second criterion is easier to apply. We shall use the formulation by Seitter and Muench (1985):

$$V = k\left[\frac{\Delta P}{\rho}\right]^{1/2}$$

where V is the speed of the density current front, ρ is the density of the warm air ahead of it, ΔP is the surface hydrostatic pressure difference between the warm air and the maximum pressure under the density current head, and k is a redefined internal Froude number which, according to Koch et al (1991), lies in the range 0.8 to 1.1. The speed of 22 m s^{-1} for the NCFR in the present study would imply a value of between 4 and 7 mb for ΔP if it had been due to a density current. Observed values of ΔP were generally close to 1 mb, with only a few values up to 2 mb. Evidently the density current mechanism was not present on this occasion, presumably because the precipitation was not sufficiently heavy or widespread.

8. Summary and discussion

Using output from an operational numerical weather prediction model, we have derived a picture of an intrusion of stratospheric air, initially with PV=2, plunging as part of a Rossby-wave breaking event down to the inversion capping the planetary boundary layer where it produced strong vertical wind shear. Vigorous turbulence at the level of the inversion is thought to have mixed some of this air into the boundary layer and to have generated strong wind gusts at the surface. The leading edge of the area of strong surface gusts was characterised by a narrow cold frontal rainband (NCFR) which is believed to have been due to shallow convection, forced by the stratospheric intrusion and enhanced in places by moist processes. The strongest evidence for the role of the stratospheric intrusion is the strip of diluted stratospheric air (with PV=1) at 2 km that appeared just behind the NCFR (and oriented parallel to it) during its most intense phase (12-15 UTC). The strength of the surface winds was due to the high velocity of the stratospheric intrusion; in fact the strongest surface gusts (35 m s^{-1}) were close to the propagation velocity of the PV anomaly. The region of PV=1 due to stratospheric air penetrating the inversion capping the boundary layer can be distinguished by its dryness from the regions of similar PV that sometimes occur in the boundary layer due to the latent heat release within frontal zones. The close relationship between this fast moving region of dry high-PV air in the low troposphere and the observed severe winds and NCFR is encouraging in terms of the implied ability of an operational NWP model to represent and anticipate such events.

The NCFR described in this paper, although superficially similar, was different from the line convection often encountered in the British Isles. Usually heavy rain from line convection is embedded within a region of lighter stratiform rain that extends rearwards into the cold air as part of an ana cold frontal circulation. Evaporation and melting of both the stratiform and convective precipitation leads to further cooling of the cold air and to the maintenance of the density current that is generally thought to drive the line convection (Browning 1986). In the present case the convective rain in the NCFR was at most only moderately heavy, and stratiform rain behind the front was absent. It seems possible, therefore, that the NCFR in this study was being driven less by precipitation processes than by the effects of the descending stratospheric intrusion. The same stratospheric intrusion was also responsible for the mainly dry secondary trough which occurred 200 km behind the primary cold front. It is beginning to be realized that density currents (Shapiro et al 1985) and line convection leading to 2-dimensional rope clouds (Shapiro and Keyser 1990) can

occur in the absence of precipitation. However, the propagation speed of the NCFR in this case was too fast to be accounted for in terms of a density current mechanism.

The case shows many similarities to another recently published event (Koch and Kocin 1991) in which a stratospheric intrusion was shown to have played an important role in generating a NCFR. They presented a complex scale-contraction process scenario whereby the strong descent of a stratospheric air mass into the lower troposphere forced the development of an isallobaric ageostrophic wind surge. According to the scenario, this wind surge frontogenetically triggered the formation of the NCFR and the resulting precipitation processes, plus orographic effects, contributed to the scale contraction process and the creation of even more severe surface winds. They, like us, noted the strong relationship between the tropopause fold behaviour and the NCFR development, including the fact that the upper-level forcing caught up with the surface front where the NCFR developed. They noted the accompanying signature in the satellite water vapour imagery and the region of strongly subsiding dry air just behind the PV fold. In particular, they also noted that the severe winds occurred behind the NCFR rather than ahead as is more usual.

One difference between the case studied by Koch and Kocin and the present one is that theirs was an anafront situation, even though the interaction of the stratospheric intrusion with the NCFR was apparently similar in other respects to the present katafront situation. Another difference is that the maximum wind gusts they observed occurred within minutes of the passage of the NCFR whereas the strongest gusts in the present study typically occurred 10 to 20 minutes (14 to 28 km) behind the NCFR. This may be attributable to the differing wetness of the fronts: only where fronts produce rather heavy precipitation are the associated diabatic processes sufficiently strong to produce surface gusts detectable above those generated by any strong upper-level forcing. Such gusts at the NCFR studied by Koch and Kocin were considered to be associated with a density current structure, a feature that was generally absent in the present case.

Acknowledgements

We are grateful to Dr P Ferris for generating various model and satellite products and to two anonymous referees for their constructive comments.

References

Browning, K.A., 1986 Conceptual models of precipitation systems. Weather and Forecasting, **1**, 23-41

Browning, K.A. and T.W. Harrold., 1970 Air motion and precipitation growth at a cold front. Quart.J.Roy.Meteor.Soc., **96**, 369-389

Browning, K.A. and C.W. Pardoe, 1973 Structure of low-level jet streams ahead of mid-latitude cold fronts. Quart.J.Roy.Meteor. Soc., **99**, 619-638

Carbone, R.E. 1982 A severe frontal rainband. Part 1: Stormwide hydrodynamic structure. J.Atmos.Sci., **39**, 258-279.

Cullen, M.J.P. 1991 The Unified Forecast/Climate Model. Short Range Forecasting Division Scientific Paper No.1, Meteorological Office, Bracknell, Berks, UK.

Hobbs, P.V. and K.R. Biswas, 1979 The cellular structure of narrow cold frontal rainbands. Quart.J.Roy.Meteor.Soc., **105**,723-727

Hoskins, B.J., M.E. McIntyre and A.W. Robertson, 1985 On the use and significance of isentropic potential vorticity maps. Quart.J.Roy.Meteor.Soc., **111**, 877-946.

Houze, R.A. Jr., P.V.Hobbs, K.R.Biswas and W.M. Davis, 1976 Mesoscale rainbands in extratropical cyclones. Mon.Wea.Rev., **104**, 868-878.

James, P.K. and K.A. Browning, 1979 Mesoscale structure of line convection at surface cold fronts. Quart.J.Roy.Meteor.Soc., **105**, 371-382.

Koch, S.E. and P.J. Kocin 1991 Frontal contraction processes leading to the formation of an intense narrow rainband. Meteor.Atmos.Phys. **46**, 123-154.

Koch, S.E., P.B. Dorian, R. Ferrare, S.H. Melfi, W.C. Skillman and D Whiteman 1991 Structure of an internal bore and dissipating gravity current as revealed by Raman Lidar.Mon.Wea.Rev., **119**, 857-887.

Parsons, D.B., C.G. Mohr and T. Gal-Chen 1987 A severe frontal rainband. Part III: Derived thermodynamic structure. J.Atmos.Sci., **44**, 1613-1631.

Sansom, H.W., 1951 A study of cold fronts over the British Isles. Quart.J.Roy.Meteor.Soc., **77**, 96-120.

Seitter, K.L. and H.S. Muench 1985 Observation of a cold front with rope cloud. Mon.Wea.Rev., **113**, 840-848.

Shapiro, M.A. and D. Keyser 1990 Fronts, jet streams and the tropopause. In Extratropical Cyclones: The Erik Palmén Memorial Volume. Eds C.W.Newton and E.O.Holopainen. Amer.Meteor.Soc., 167-191.

Shapiro, M.A., T. Hampel, D.Rotzoll and F.Mosher 1985 The frontal hydraulic head: a micro-alpha scale (~1km) triggering mechanism for mesoconvective weather systems. Mon.Wea.Rev.,**113** ,1166-1183.

Smith, R.K. and M.J.Reeder 1988 On the movement and low-level structure of cold fronts. Mon.Wea.Rev., **116**, 1927-1944.

Thorncroft, C.D., B.J.Hoskins and M.E.McIntyre 1993 Two paradigms of baroclinic-wave life cycle behaviour. Quart.J.Roy.Meteor.Soc., **119**, In press.

Figure Legends

Fig 1. Surface analysis at 12 UTC, 23 December 1991, from the Central Forecasting Office of the Meteorological Office.

Fig 2. Infra-red imagery from NOAA 11 at 1408 UTC, 23 December 1991 (Photograph from the University of Dundee).

Fig 3. (a) Composite weather radar network display for 1230 UTC, 23 December 1991 at a time when the narrow cold frontal rainband (NCFR) was most intense. Colours represent rainfall intensity averaged over 5 km squares from >0.1 mm h^{-1} (blue) to >16 mm h^{-1} (brown). (b) shows the progression of the NCFR at 1-hour intervals. The limit of good radar coverage is shown by the dashed line. The structure of the rainband was unclear in the region covered by the figure title.

Fig 4. Zoomed Meteostat infra-red image for 12 UTC, 23 December 1991, showing details of the cloud top temperature close to the tops of the NCFR. Temperatures below +2, 0 and -2°C are shown as shades of light grey. Tops colder than -4°C are shown white. Cloud, land and sea surfaces warmer than +2°C are dark grey. The narrow (<100 km) band of shallow cloud responsible for the NCFR extends from just south of the Wash to Portland Bill and then west-southwestwards to the south of Cornwall.

Fig 5. Output from the lowest uncluttered beams of the Chenies (London) radar at 1230 UTC, 23 December 1991, showing surface rainfall associated with the NCFR, averaged over 2 km, out to a range of 75 km. Dotted line >0.1mm h^{-1}. Hatched shading > 4mm h^{-1}. Solid shading > 16 mm h^{-1}.

Fig 6. Anemograph traces (a) for Wittering (52°37'N 00°28'W) characteristic of the passage of the two wind surges behind the NCFR on 23 December 1991, and (b) for a station experiencing line convection associated with an ana cold front, taken from James and Browning (1979). The starts of the wind veers associated with the first (major) and second (minor) wind surge are marked by arrows in (a). The brief burst of precipitation associated with the NCFR on 23 December occurred at 1150 UTC, 20 minutes before the peak gust associated with the first wind surge.

Fig 7. Gusts in excess of 55 knots on 23 December 1991. The numbers give end of each hour during which gusts were recorded. Solid lines enclose recorded gusts for the hours ending 9, 12, 15 and 18 UTC for comparison with Fig 13(c).

Fig 8. Surface weather associated with (a) the primary cold front and (b) the secondary trough on 23 December 1991, derived from autographic records over the British Isles and from hourly synoptic observations over continental Europe. Isochrones in (a) and (b) relate to the start of the two main periods of wind veer. Station plots show magnitude of veer (in degrees)(top left), maximum gust (knots)(top right), change in relative humidity (percent)(bottom right), and change in temperature (deg C)(bottom left). For data derived from autographic records, the wind veer is underlined where it took place in less than 20 min and overlined where the veer briefly overshot during the period of the wind surge. Station plots are open and singly or doubly encircled (autographic records only) according to whether the wind surge was accompanied by no rain, light rain, or heavier rain in excess of 4 mm h^{-1} averaged over 20 mins. A broken circle indicates that the occurrence of rain has been inferred from radar alone.

Fig 9. Vertical section transverse to the NCFR at 12 UTC, 23 December 1991, derived from the Unified Model. The position of the section (T_{12} T_{12}) is shown in Fig 10 (c).

Key to (a): relative humidity (solid contours for 10, 30, 50, 70 and 90%; stippled >50%).

vertical velocity (dashed contours at 2 cm s^{-1} intervals).

NCFR (vertical arrow up to 730 mb).

Key to (b): wet bulb potential temperature (solid contours at 2°C intervals).

absolute vorticity (dashed contours for 15, 20 and 25 x $10^{-5}s^{-1}$); stippled >15 x $10^{-5}s^{-1}$).

Key to (c) potential vorticity (thick solid line = 2 PV units).

transverse wind component relative to NCFR (solid contours at 10 m s^{-1} intervals; stippled for winds overtaking the NCFR).

wind component parallel to the NCFR (bold dashed contours at 10m s^{-1} intervals)

dry bulb potential temperature (short dashed contours at 5°C intervals).

Fig 10. Analyses on the 300K isentropic surface at 00, 06 and 12 UTC, 23 December 1991, derived from the Unified Model.

(a, b, c): potential vorticity (isopleths for PV = 1 and 2).

(d, e, f): relative humidity (solid contours for 30 and 70%; stippled >30%).

areas of rather strong descent (dashed contours for -2 and -4 cm s^{-1})

axis of PV filament (thick solid line)

(g, h, i): streamlines of flow relative to PV filament (solid lines).

geopotential height (dashed contours at 1 km intervals).

axis of PV filament (thick solid line).

The orientations of cross sections in Figs 9 and 12 are shown in (a) and (c). The orientation of the segmented section in Fig 11, along the axis of the PV filament, is shown in (c) by the dashed line whose endpoints are labelled PP. The model-derived axis of maximum relative humidity at 800 mb, related to the surface cold front, is shown dotted in (a), (b) and (c).

Fig 11. Vertical section along the axis of the filament of high potential vorticity at 12 UTC, 23 December 1991, derived from the Unified Model. The location of the section, PPPPP, is shown in Fig 10 (c). Thick solid lines represent potential vorticity at intervals of 1 PV unit. Thin solid lines represent relative humidity (30, 50 and 70%). Dashed lines represent dry bulb potential temperature at intervals of 10K. The position of the section in Figs 9 (a) and 12(b) is also shown (T_{12} T_{12}).

Fig 12. Vertical sections transverse to the NCFR at (a) OO UTC and (b) 12 UTC, 23 December 1991, derived from the Unified Model. The positions of the sections, T_oT_o and $T_{12}T_{12}$, are shown in Figs 10 (a) and 10(c), respectively.

Key: dynamical tropopause (thick solid line = 2 PV units).

regions of most strongly descending air and ascending air (stippled for descent in excess of 4 cm s^{-1} and vertically hatched for ascent in excess of 2 cm s^{-1})

nearly saturated air (horizontally hatched shading >90%).

frontal shear zone (dashed lines for V=10, 20 and 30 m s^{-1})

warm air advection (dotted contour)

upper level jet maximum (J).

Fig 13. Successive positions, on 23 December 1991, of the lowermost portions of the stratospheric intrusion as represented by PV=2 in the free troposphere and PV=1 near the top of the boundary layer.

(a) Geopotential height of PV=2

(b) Extent of PV=2 at 3 km

(c) Extent of PV=1 at 2 km

Fig 14. Tephigram for 12 UTC, 23 December 1991, showing dry bulb and dew point temperature profiles at Camborne, 50 km behind the primary cold front and NCFR. Winds are plotted on the right; thick, long and short barbs, respectively, represent 25, 5 and 2.5 m s^{-1} (50, 10 and 5 knots).

Fig 15. Meteostat water vapour imagery at (a) 06, (b) 09, (c) 12 and (d) 15 UTC, 23 December 1991 (Courtesy EUMETSAT). Dark zones correspond to dry air in the upper and middle troposphere. The area of geographical coverage is clarified in (e) which also shows successive positions of the centre (large dots) and leading edge (short lines) of the dark zone associated with the stratospheric intrusion.

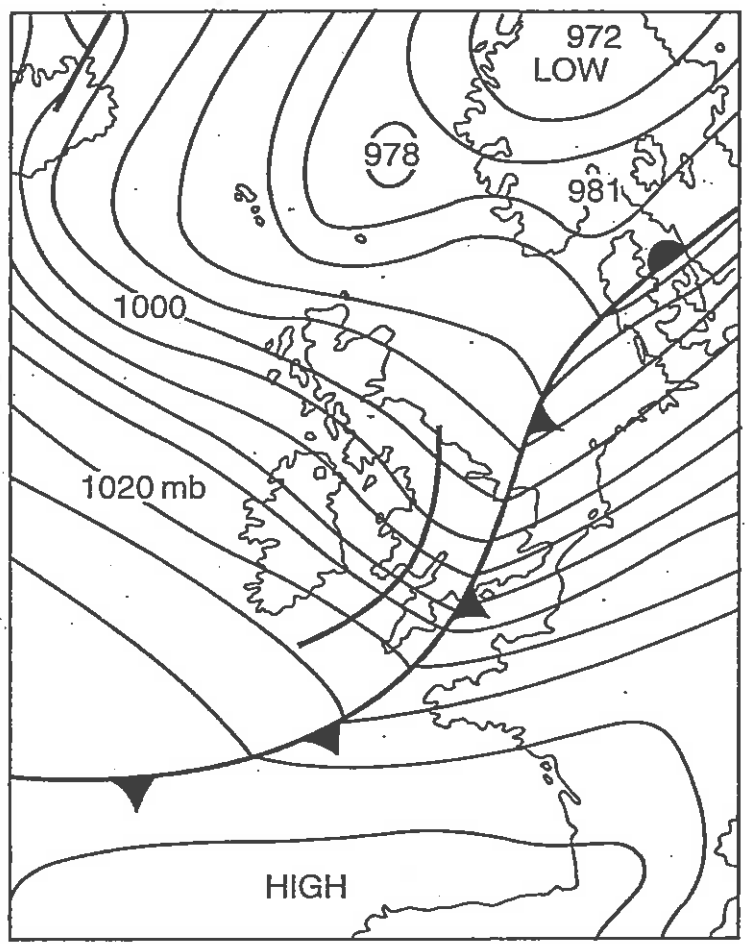

Fig 1

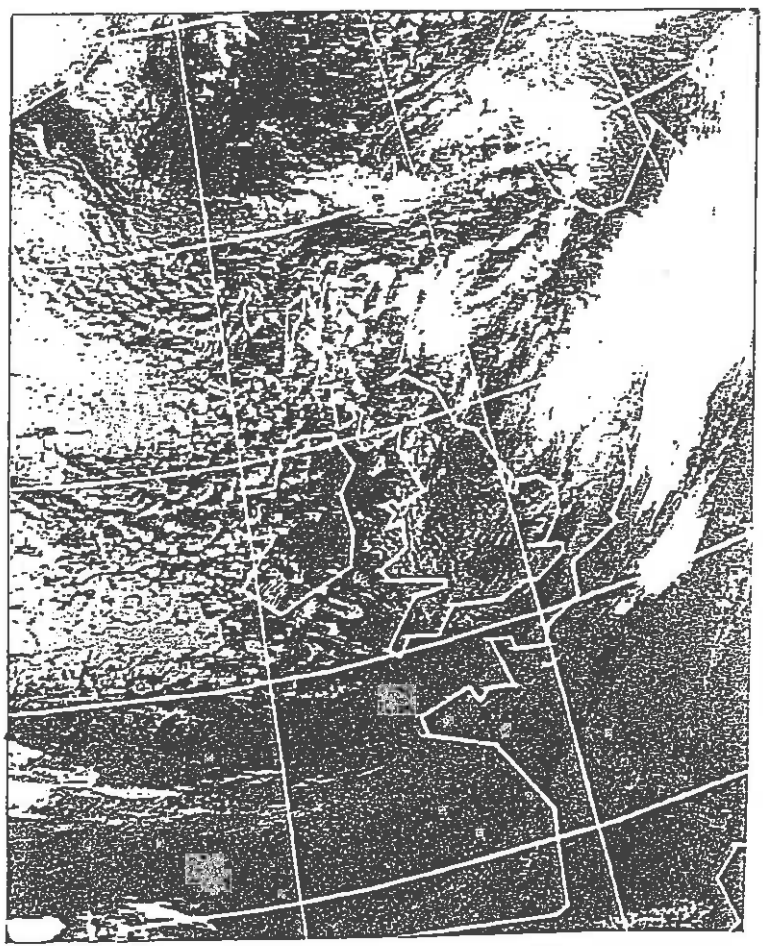

Fig 2

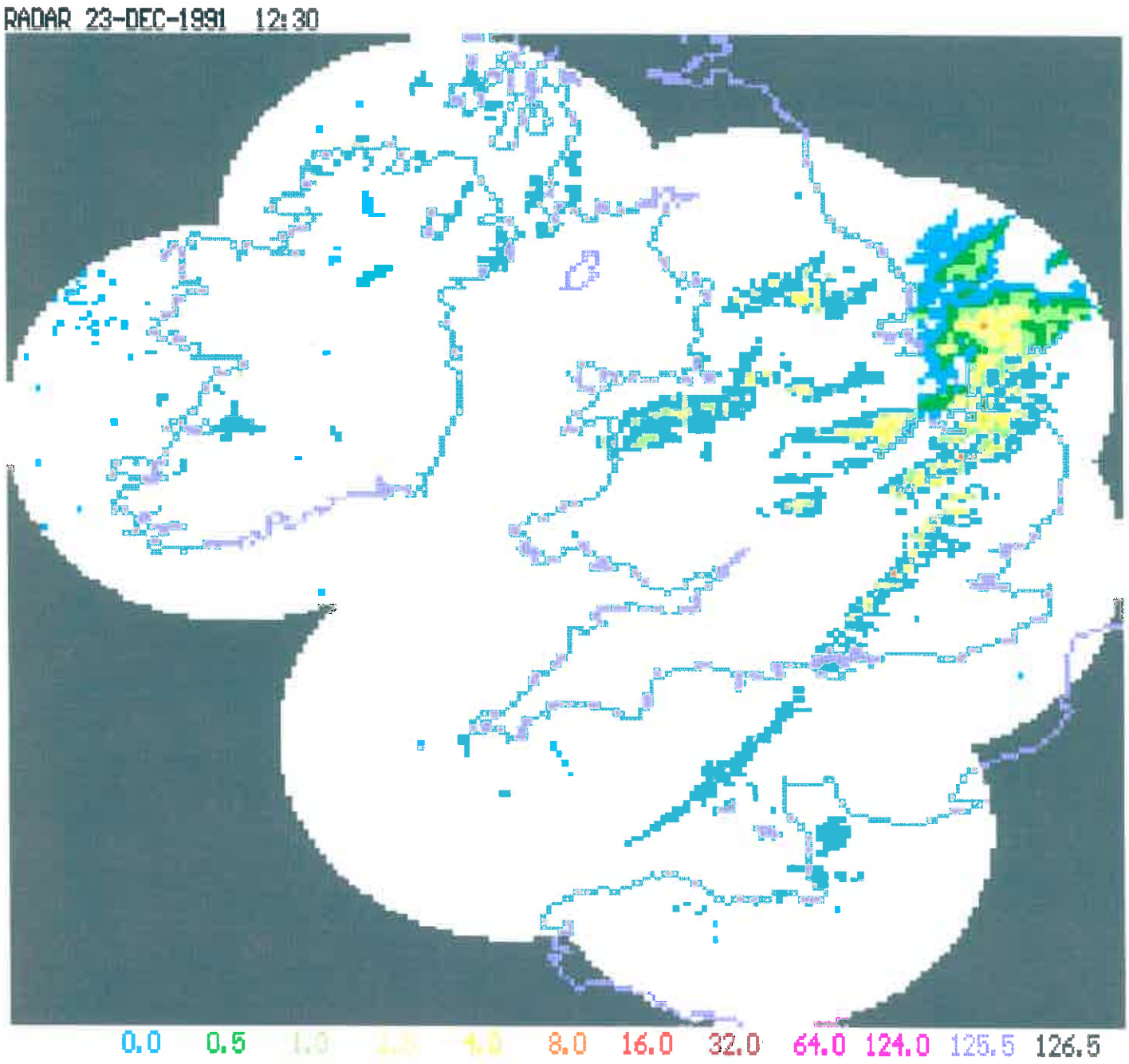

Fig 3(a)

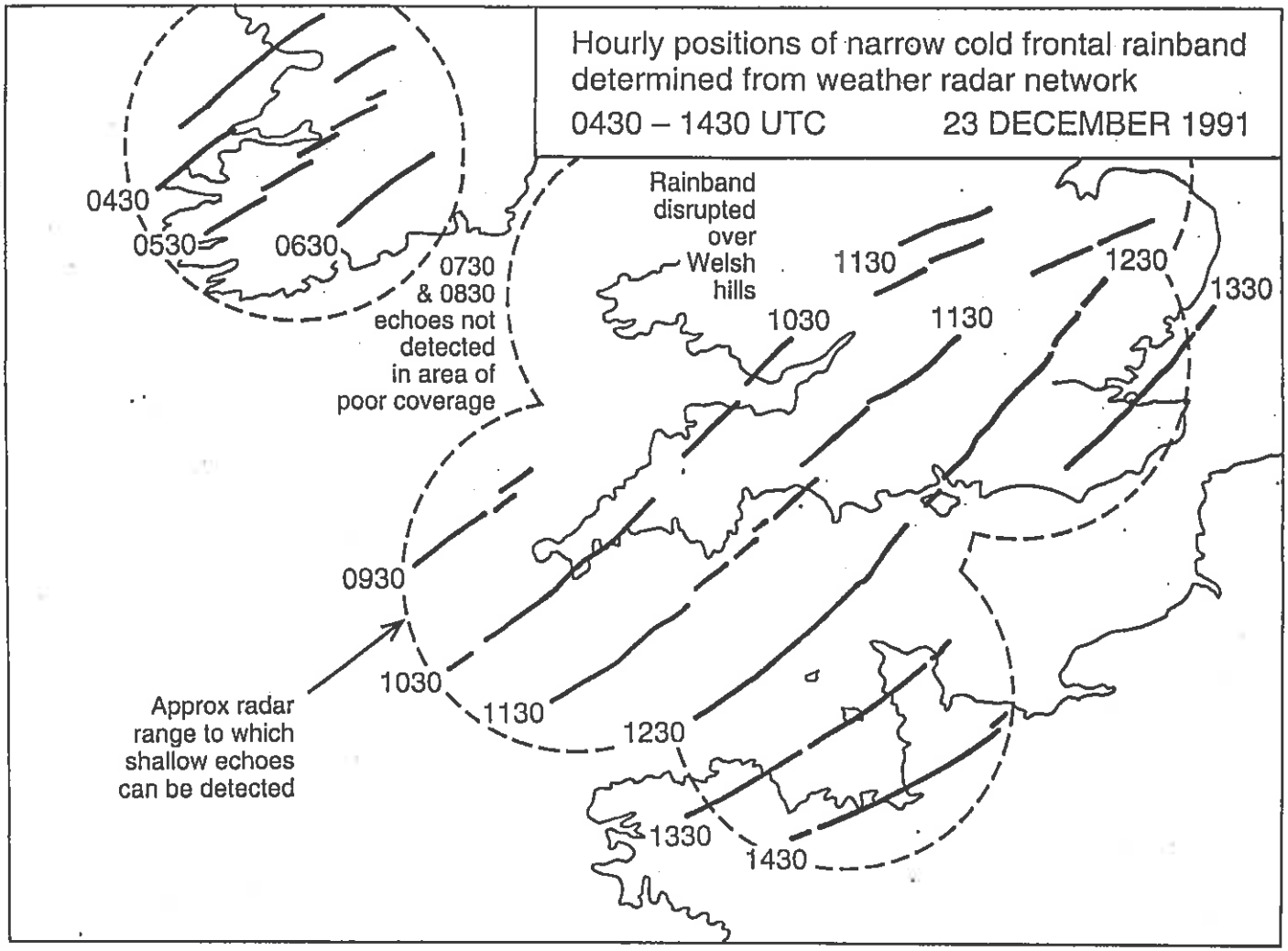
Hourly positions of narrow cold frontal rainband determined from weather radar network
0430 – 1430 UTC 23 DECEMBER 1991
0430
0530
0630
0730 & 0830 echoes not detected in area of poor coverage
Rainband disrupted over Welsh hills
1030
1130
1230
1330
0930
1030
1130
1230
1330
1430
Approx radar range to which shallow echoes can be detected

Fig 3(b)

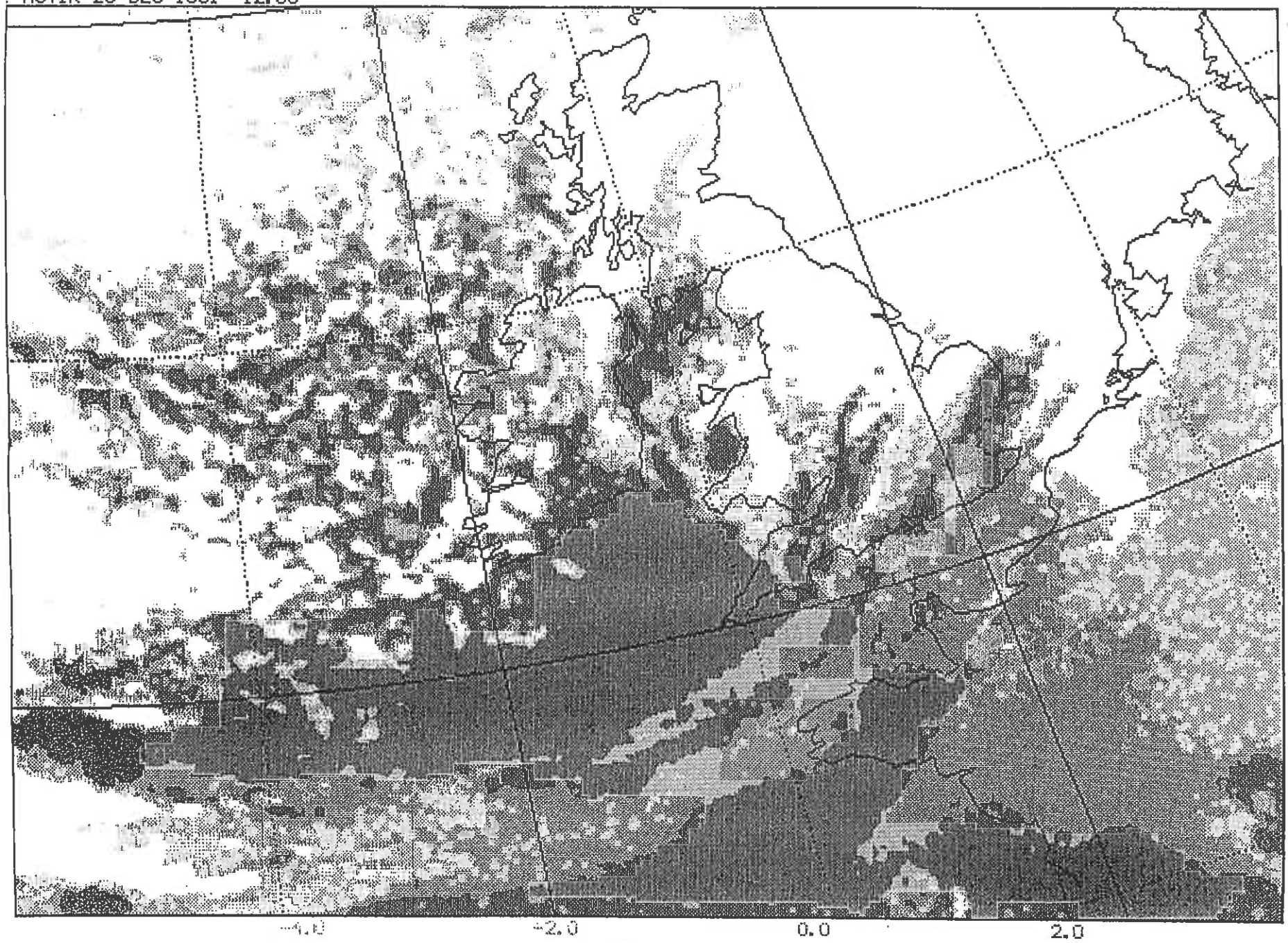

Fig 4

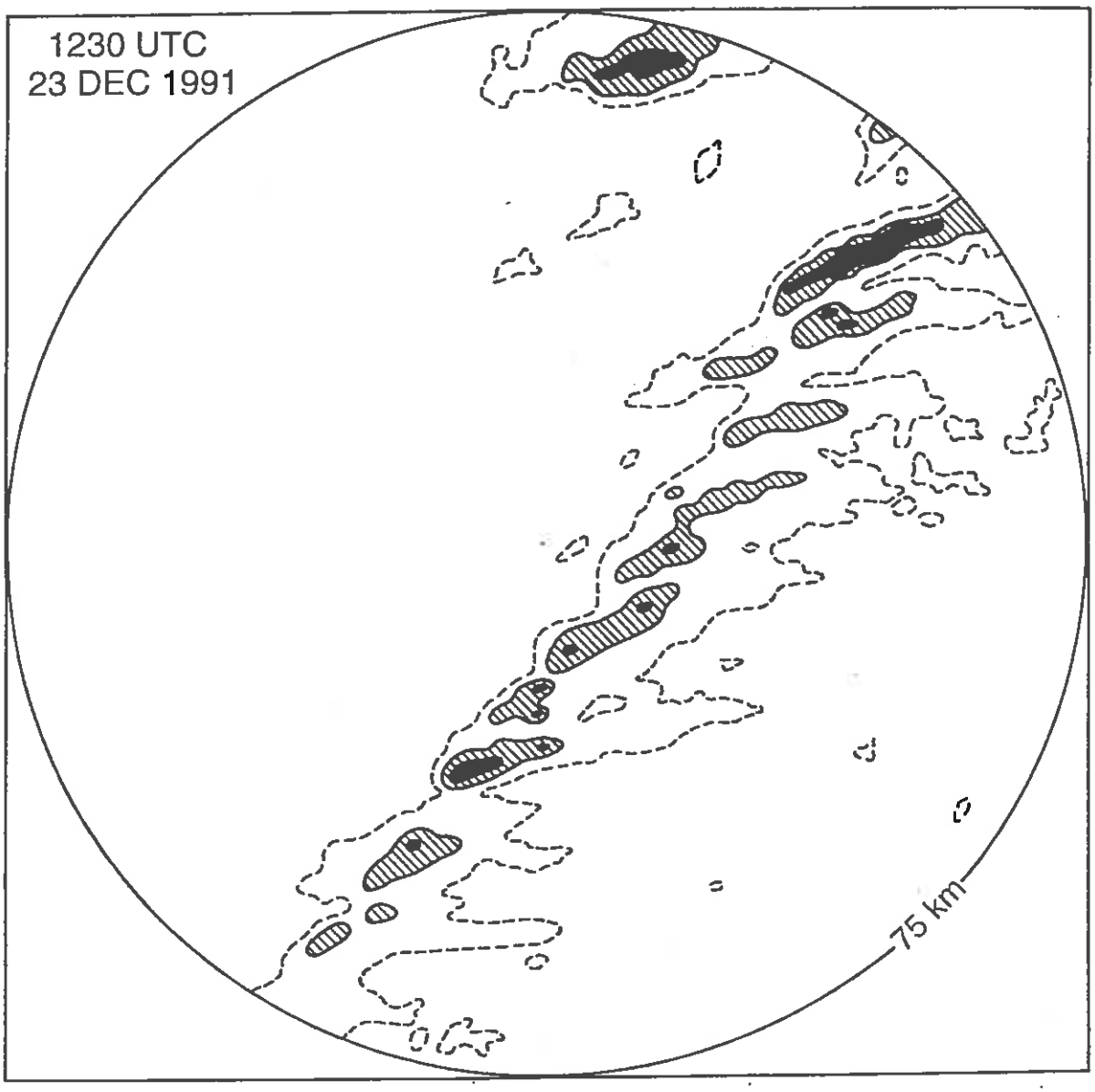

Fig 5

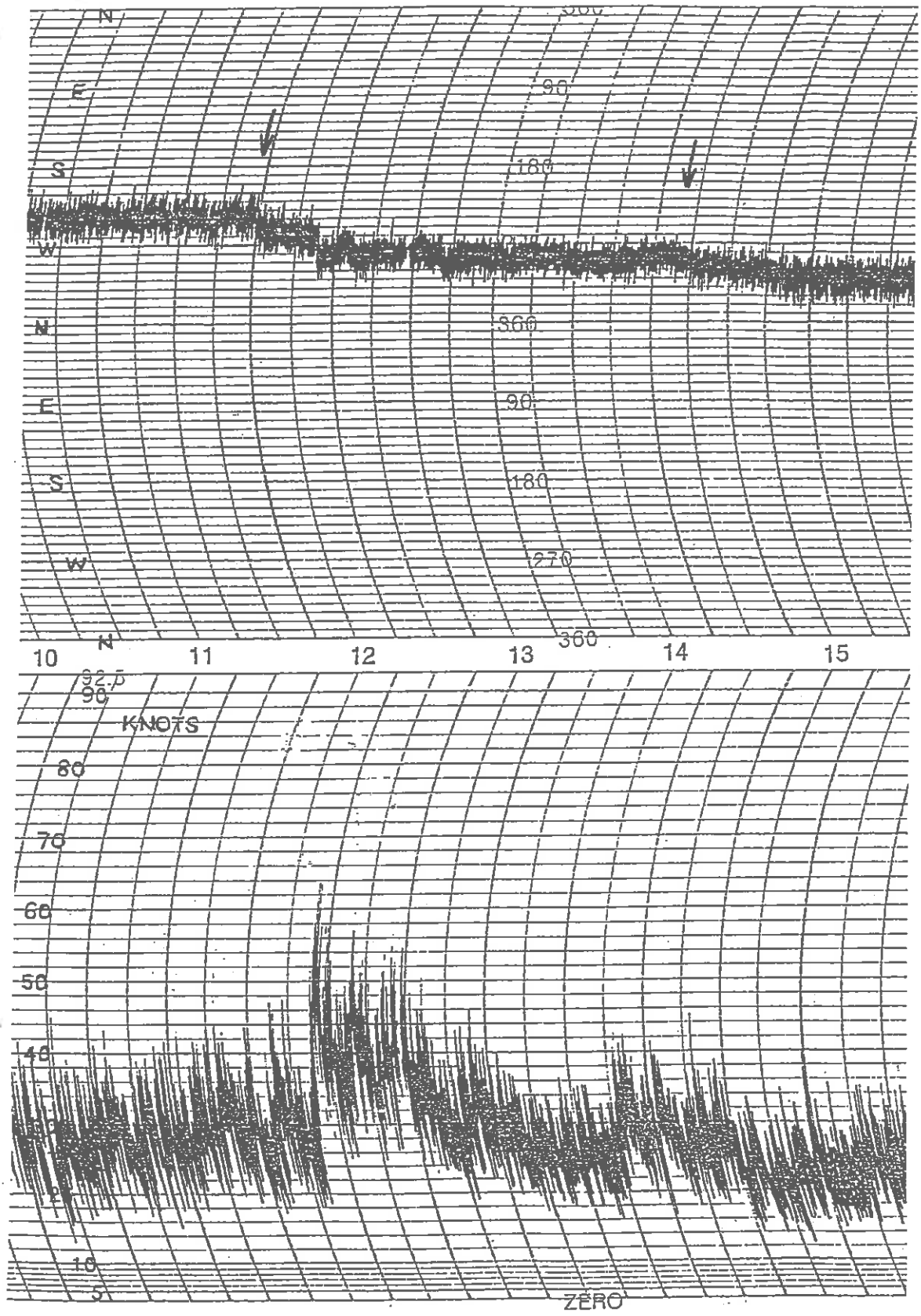
N
E
S
W
90
180
360
270
10
11
12
13
14
15
KNOTS
80
70
60
50
40
30
20
10
5
ZERO

Fig 6(a)

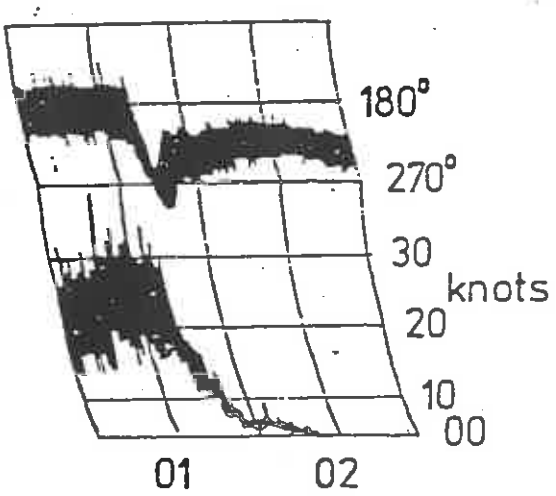

Fig 6(b)

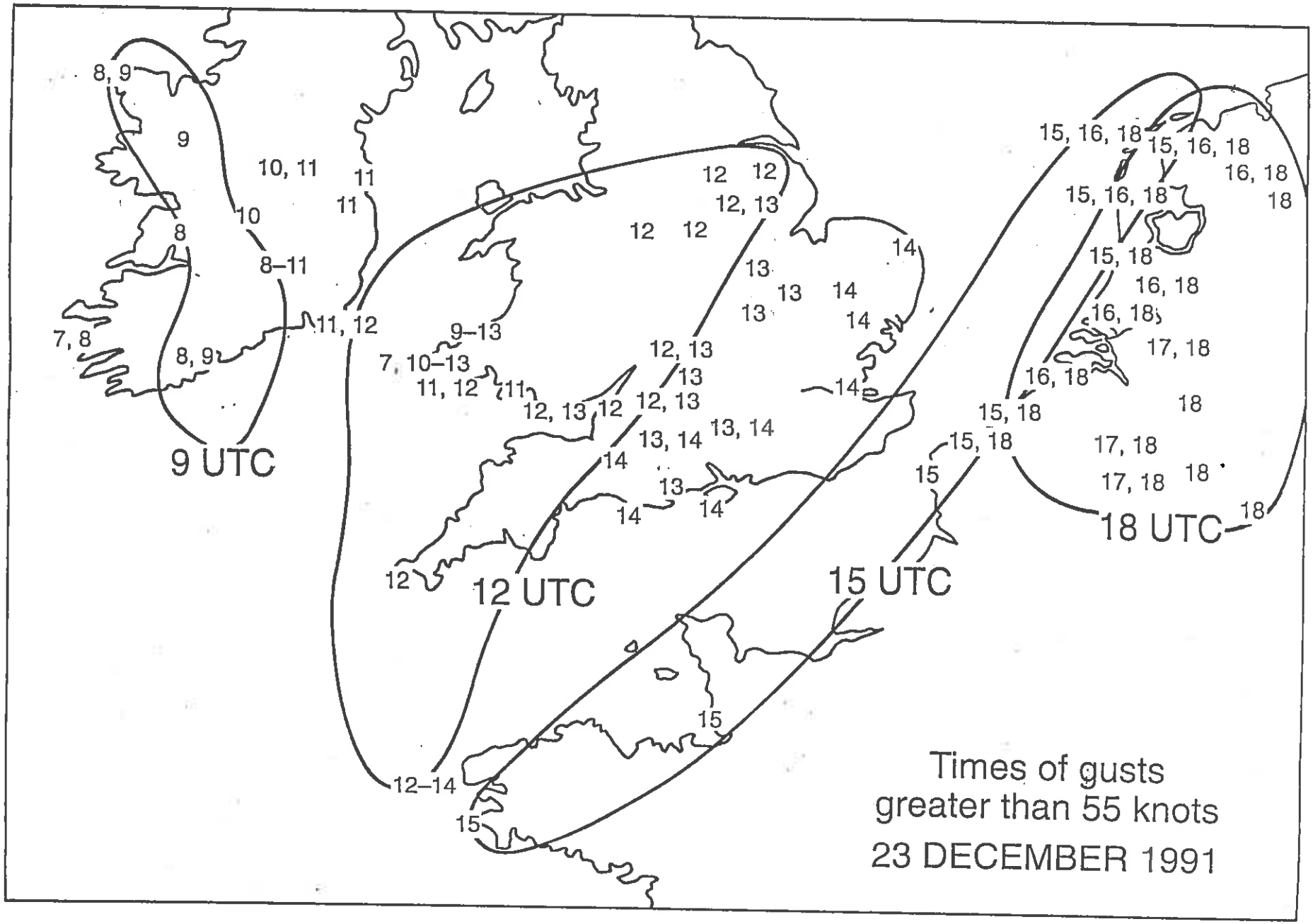
8, 9
9
10, 11
11
11
10
8
8–11
7, 8
8, 9
11, 12
9–13
7, 10–13
11, 12
11
12, 13
12
12, 13
13, 14
13, 14
14
13
14
12
9 UTC
12 UTC
12
12
12
12, 13
13
13
14
14
12, 13
12, 13
13
14
14
13
14
12–14
15
15
15
15, 16, 18
15, 16, 18
16, 18
15, 16, 18
18
15, 18
16, 18
16, 18
17, 18
16, 18
18
15, 18
15, 18
17, 18
15
17, 18
18
18
18 UTC
15 UTC
Times of gusts
greater than 55 knots
23 DECEMBER 1991

Fig 7

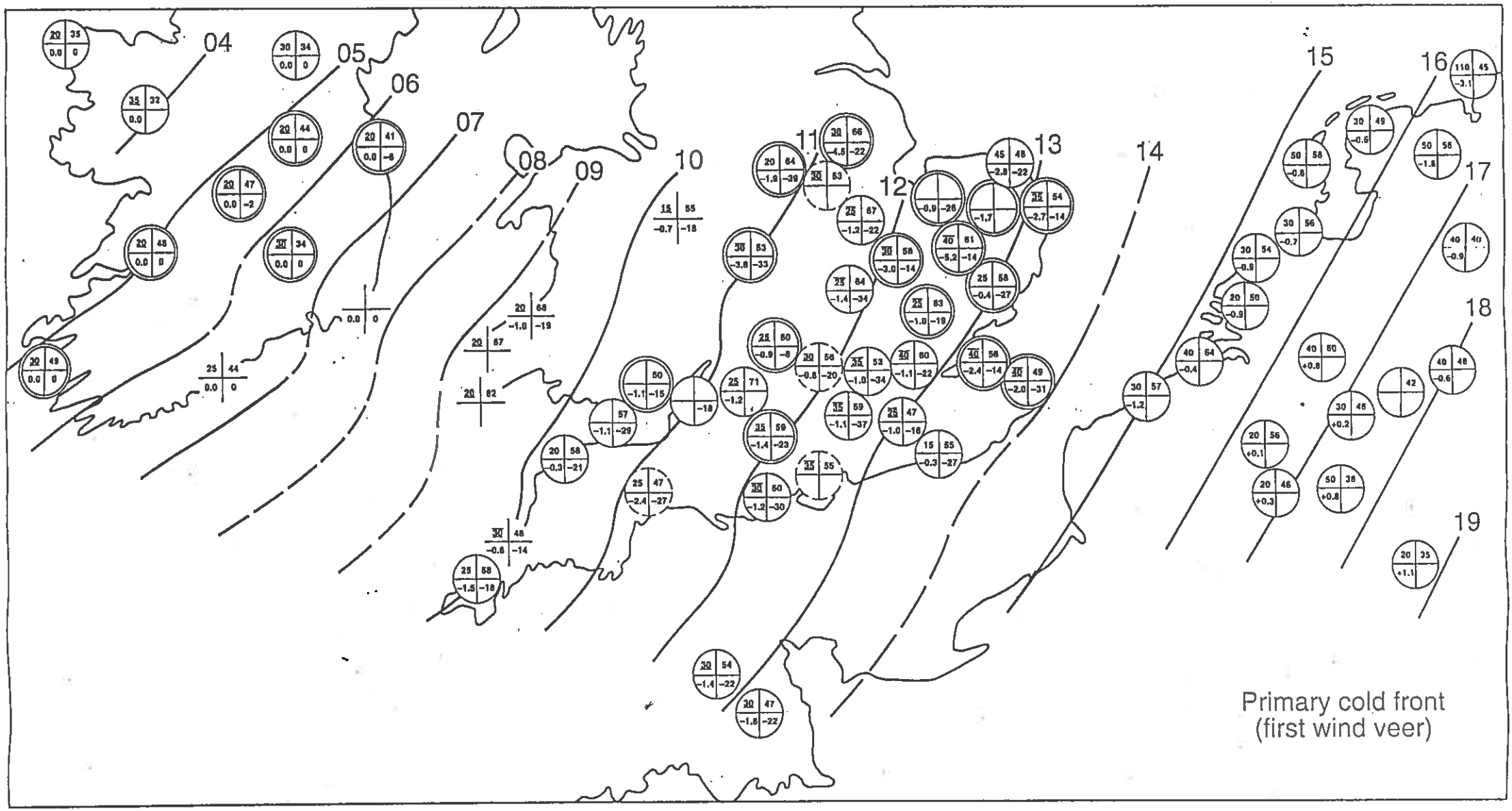
04
05
06
07
08
09
10
11
12
13
14
15
16
17
18
19
Primary cold front
(first wind veer)

Fig 8(a)

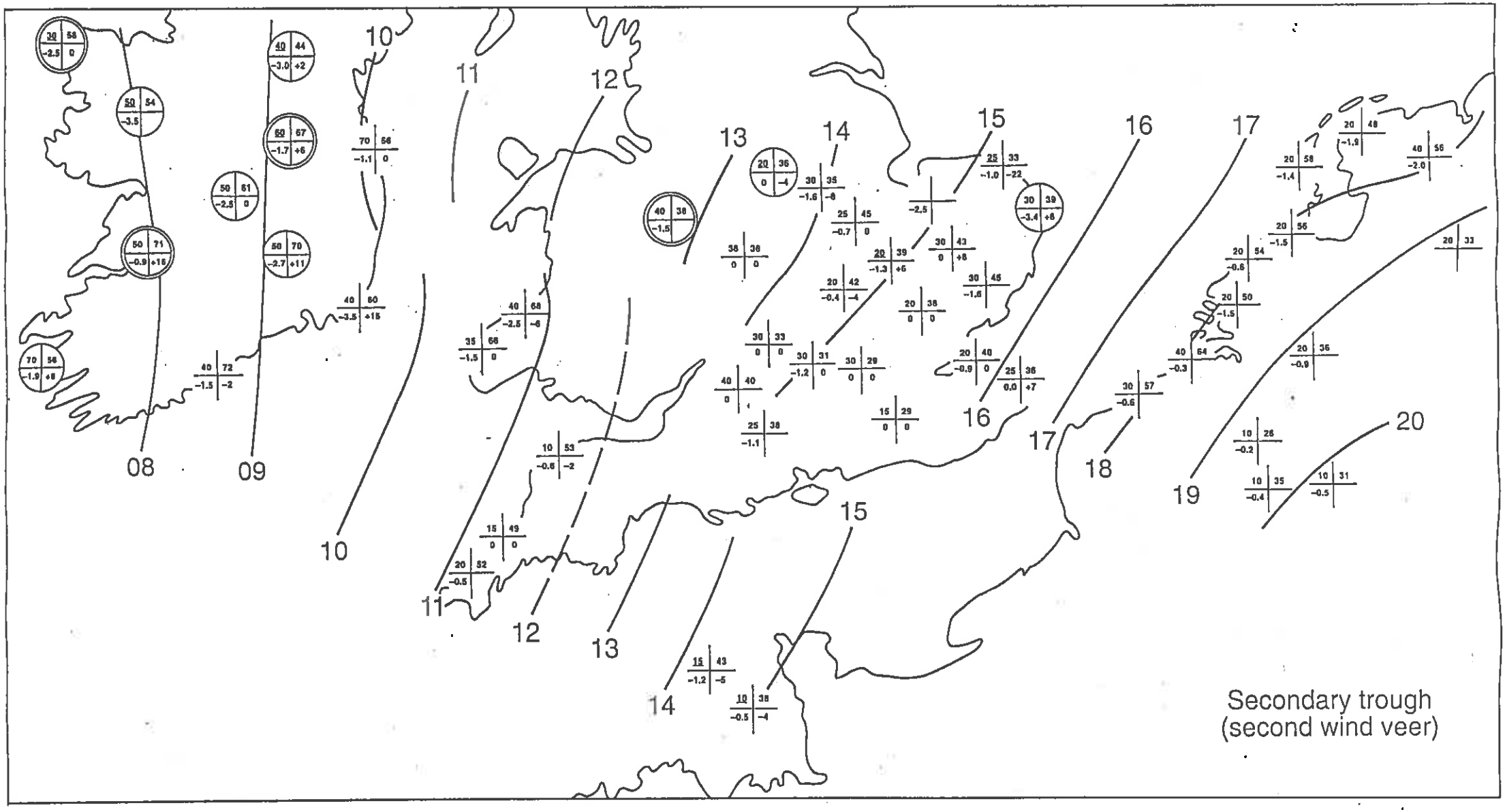
08
09
10
11
12
13
14
15
16
17
18
19
20
Secondary trough
(second wind veer)

Fig 8(b)

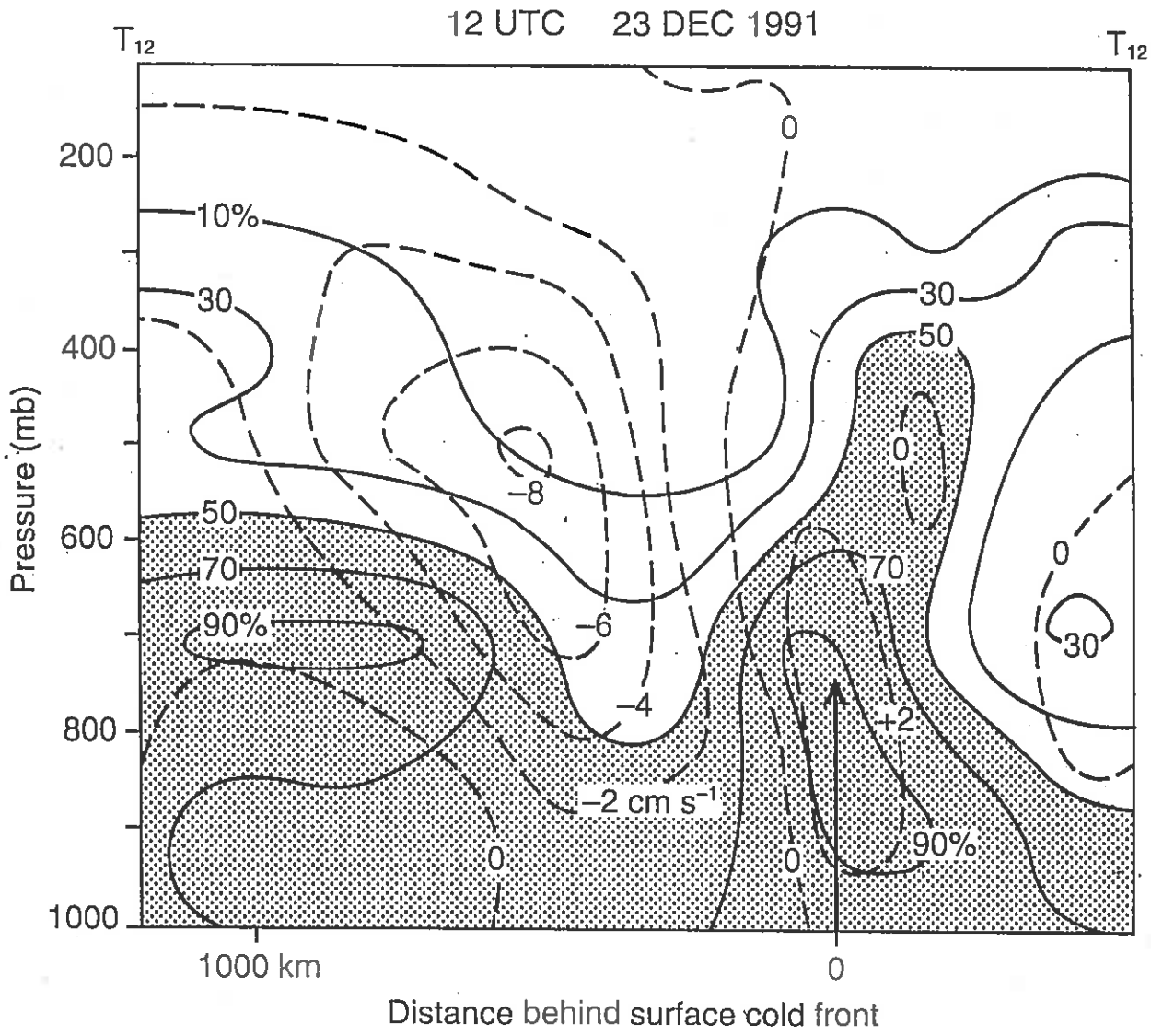
12 UTC 23 DEC 1991
T_{12}
T_{12}
200
400
600
800
1000
Pressure (mb)
10%
30
50
70
90%
0
-8
-6
-4
-2 cm s^{-1}
+2
1000 km
0
Distance behind surface cold front

Fig 9(a)

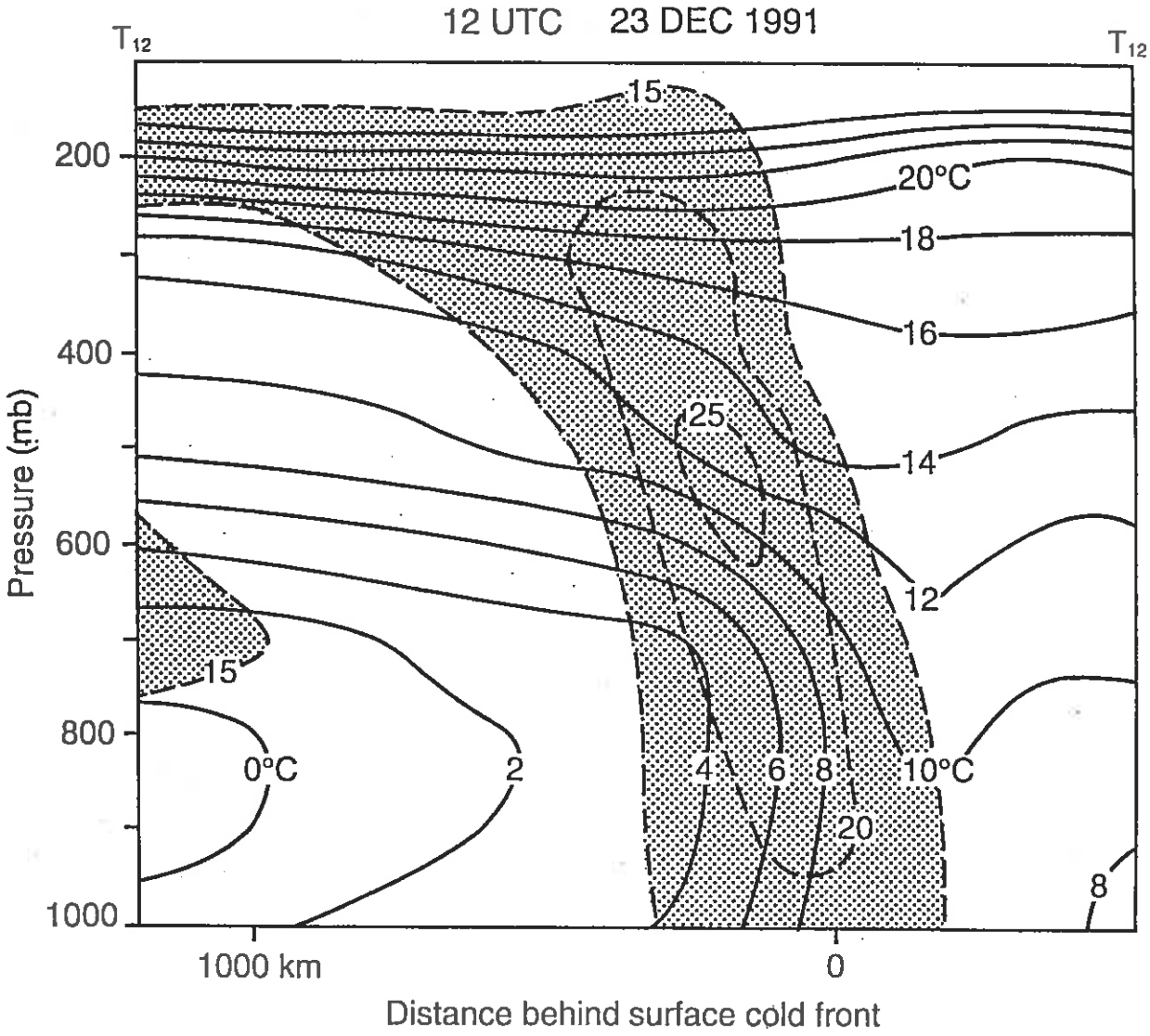
12 UTC 23 DEC 1991
T12
T12
15
20°C
18
16
25
14
12
15
0°C
2
4
6
8
10°C
20
8
200
400
600
800
1000
Pressure (mb)
1000 km
0
Distance behind surface cold front

Fig 9(b)

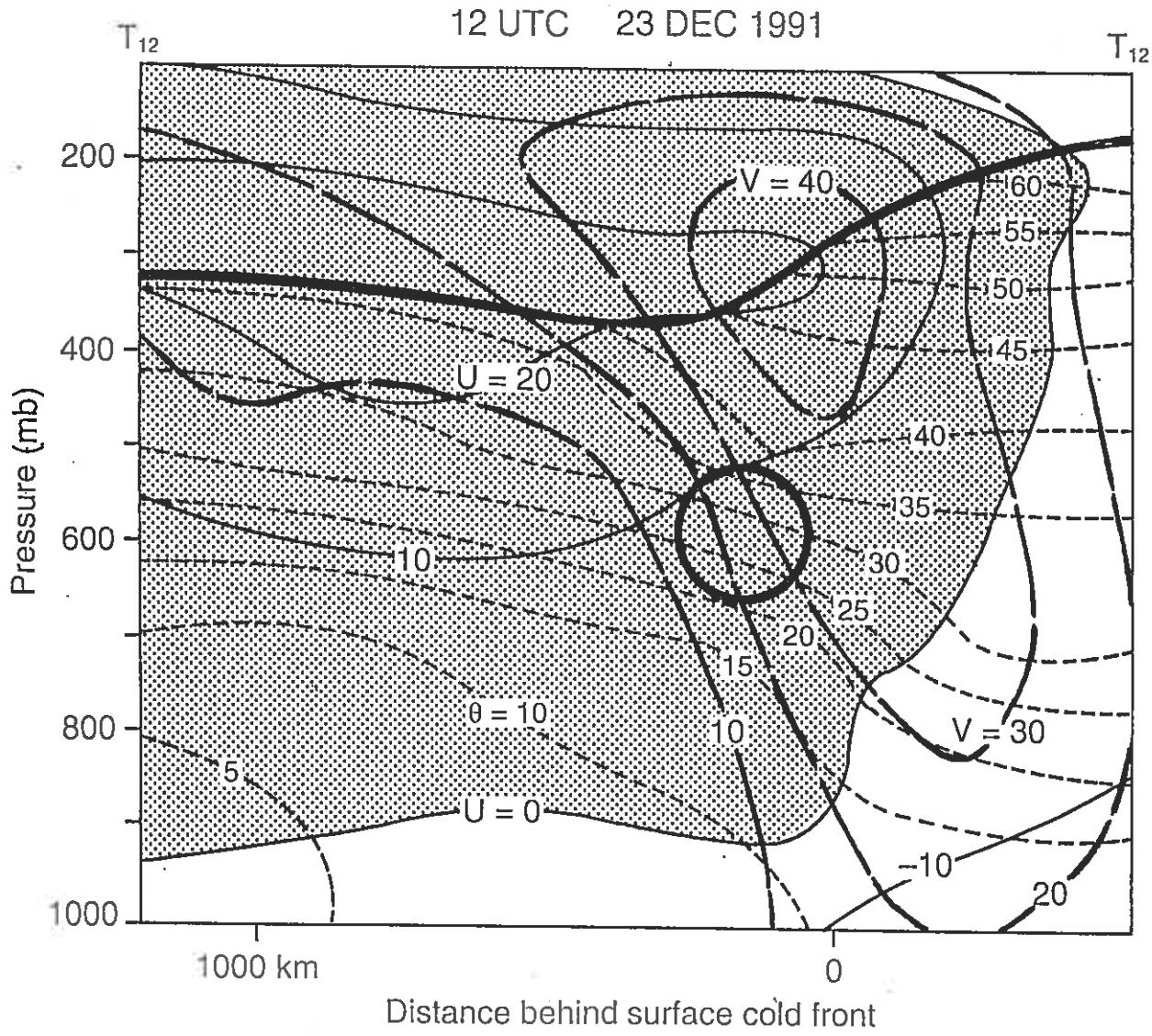
12 UTC 23 DEC 1991
T12
T12
200
400
600
800
1000
Pressure (mb)
V = 40
60
55
50
45
40
35
30
25
20
15
10
U = 20
10
θ = 10
5
U = 0
V = 30
−10
20
1000 km
0
Distance behind surface cold front

Fig 9(c)

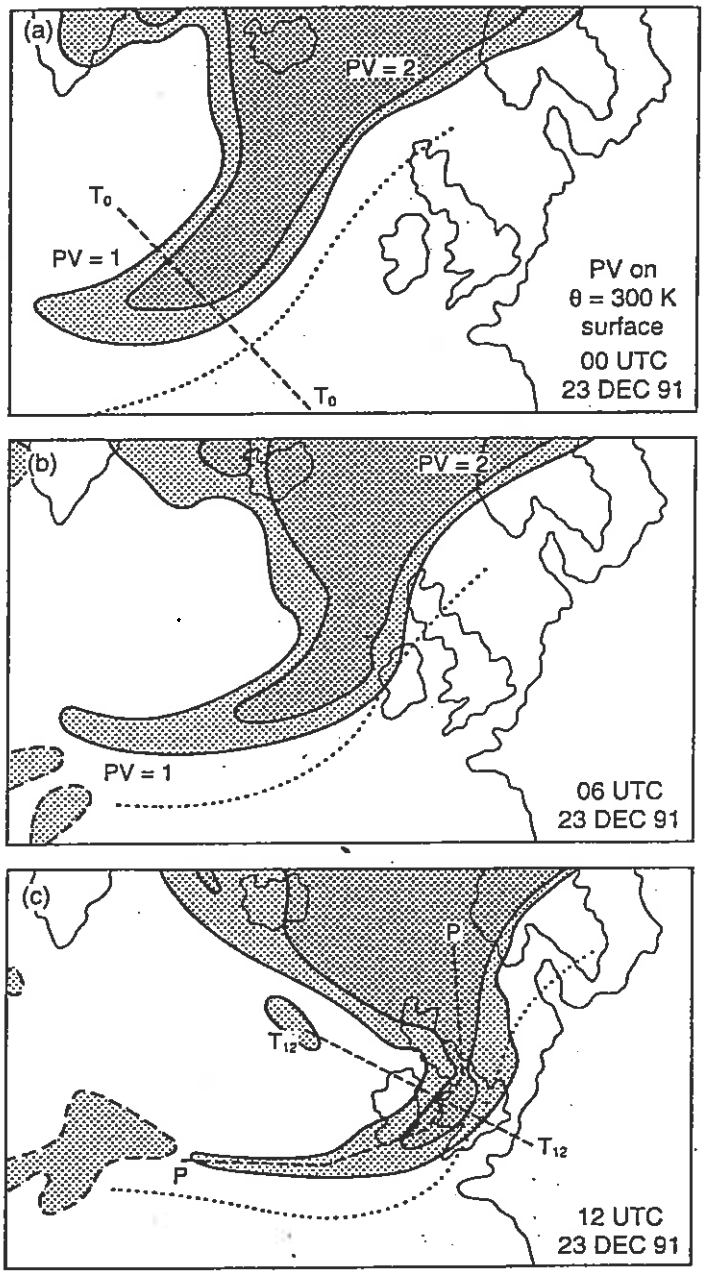
(a)
PV = 2
T_0
PV = 1
T_0
PV on
θ = 300 K
surface
00 UTC
23 DEC 91
(b)
PV = 2
PV = 1
06 UTC
23 DEC 91
(c)
P
T_{12}
T_{12}
P
12 UTC
23 DEC 91

Fig 10 a
b
c

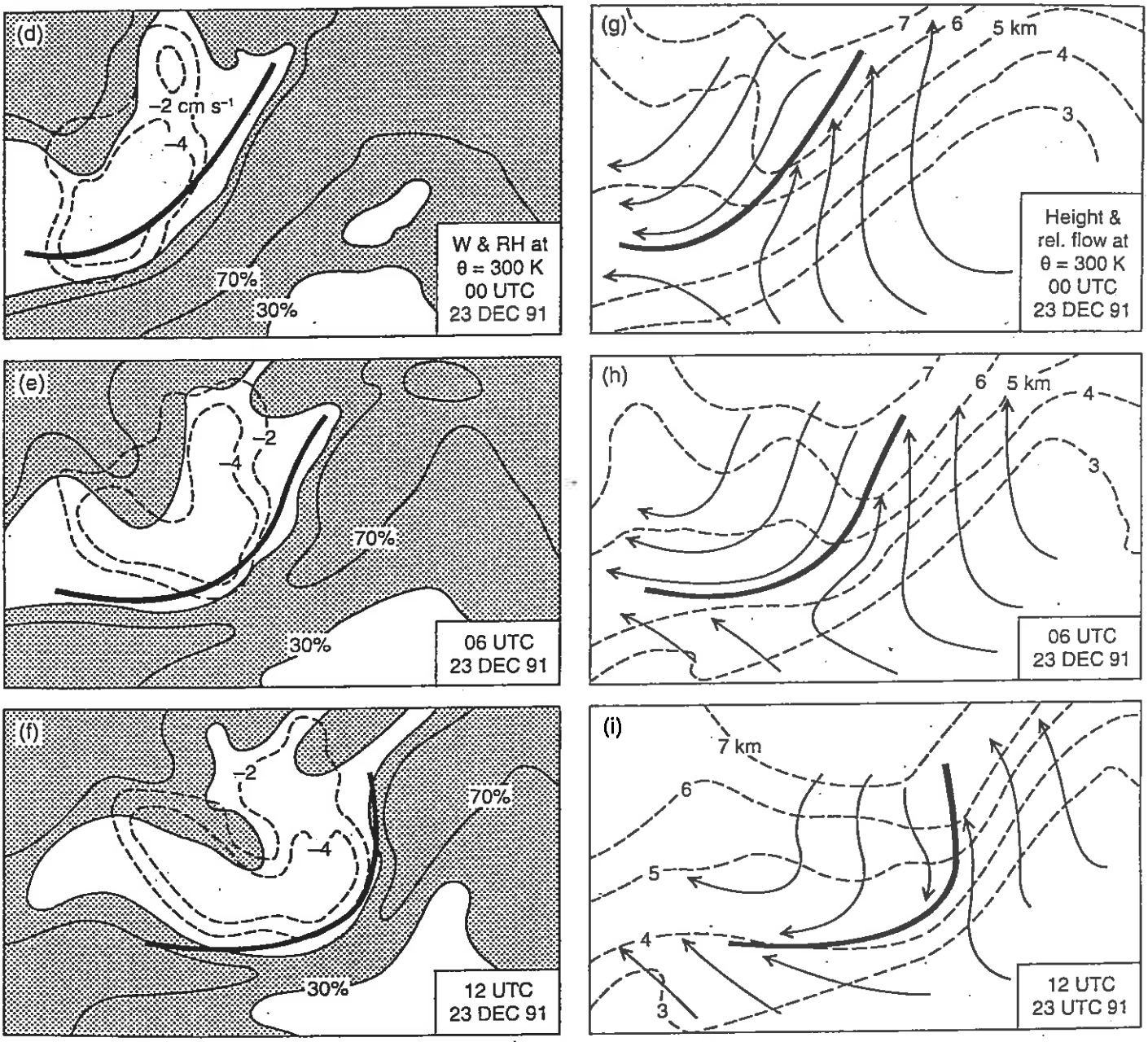

Fig 10 d g
e h
f i

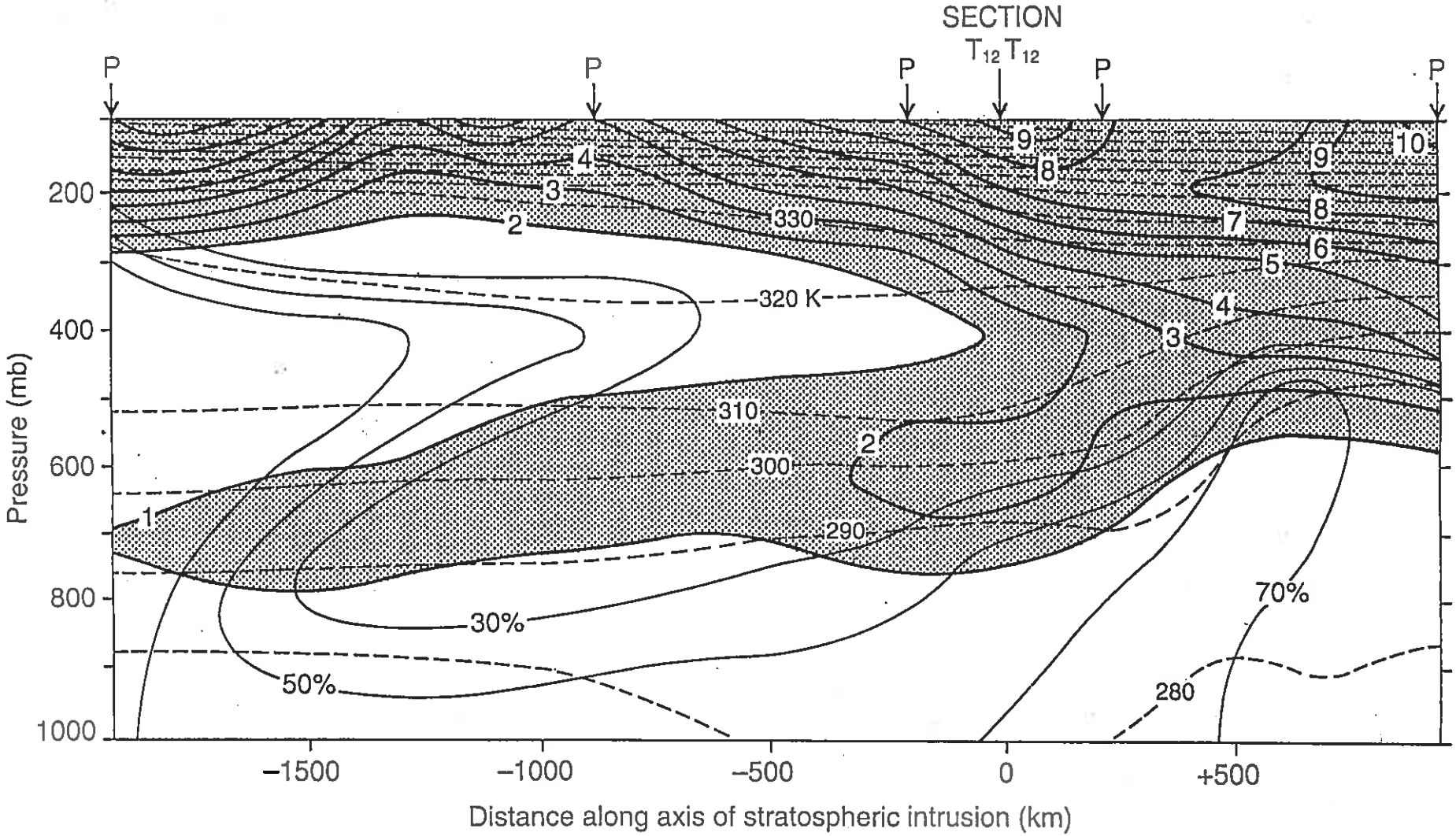
SECTION
T_{12} T_{12}
P
P
P
P
P
200
400
600
800
1000
Pressure (mb)
320 K
310
300
290
330
280
70%
30%
50%
−1500
−1000
−500
0
+500
Distance along axis of stratospheric intrusion (km)

Fig 11

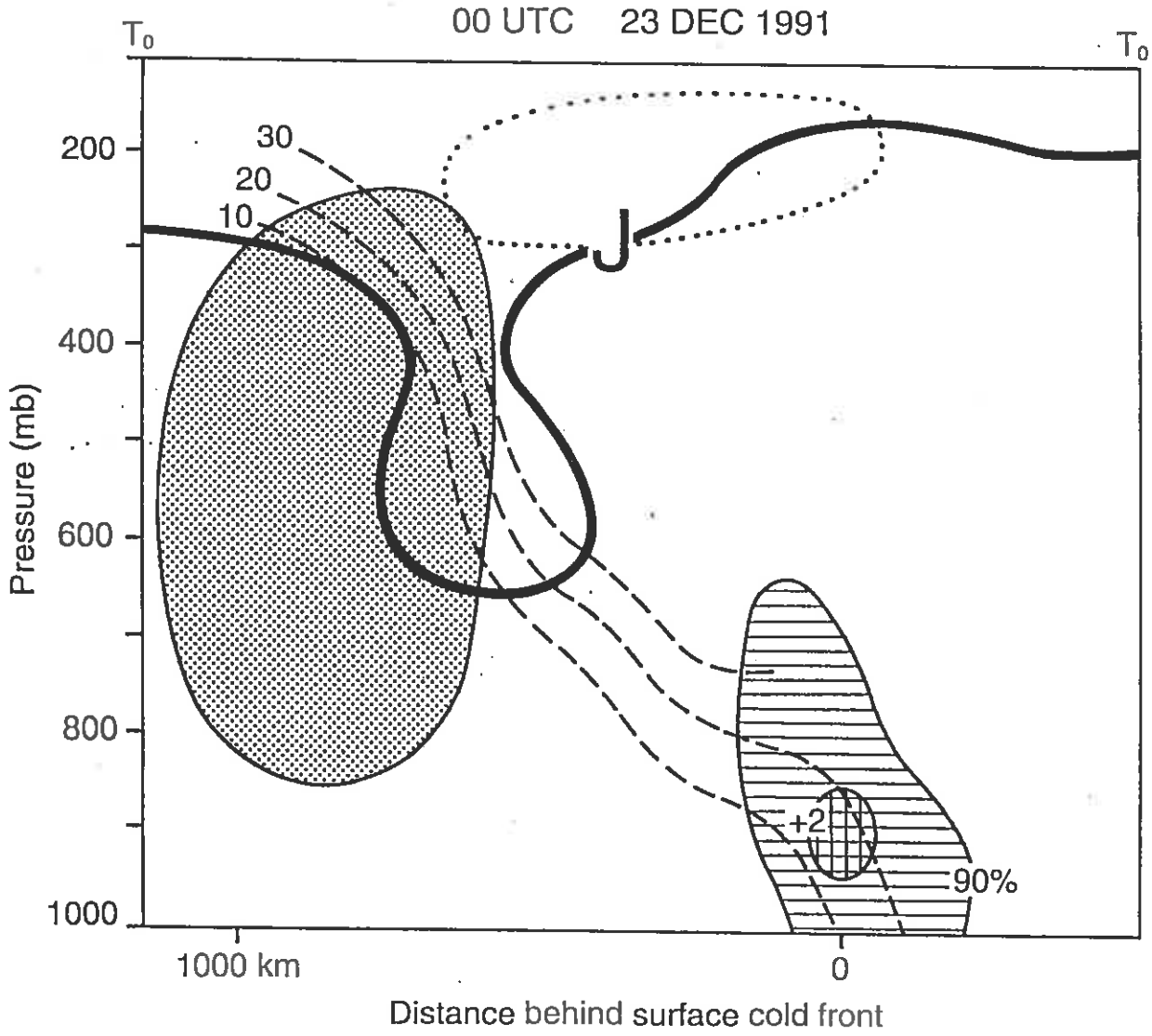
00 UTC 23 DEC 1991
T_0
T_0
200
400
600
800
1000
Pressure (mb)
30
20
10
J
+2
90%
1000 km
0
Distance behind surface cold front

Fig 12(a)

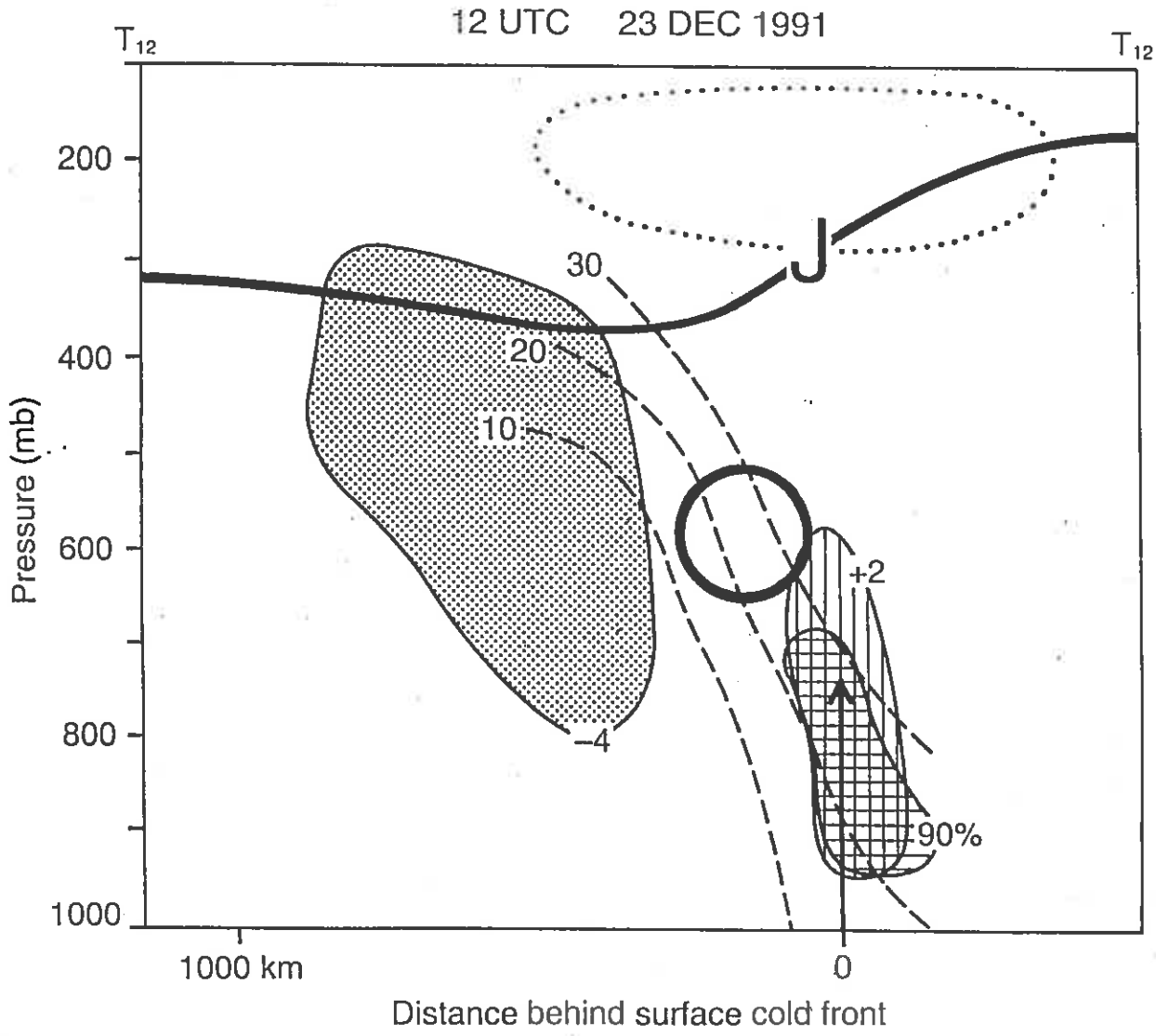
12 UTC 23 DEC 1991
T_{12}
T_{12}
200
400
600
800
1000
Pressure (mb)
30
20
10
−4
+2
90%
1000 km
0
Distance behind surface cold front

Fig 12(b)

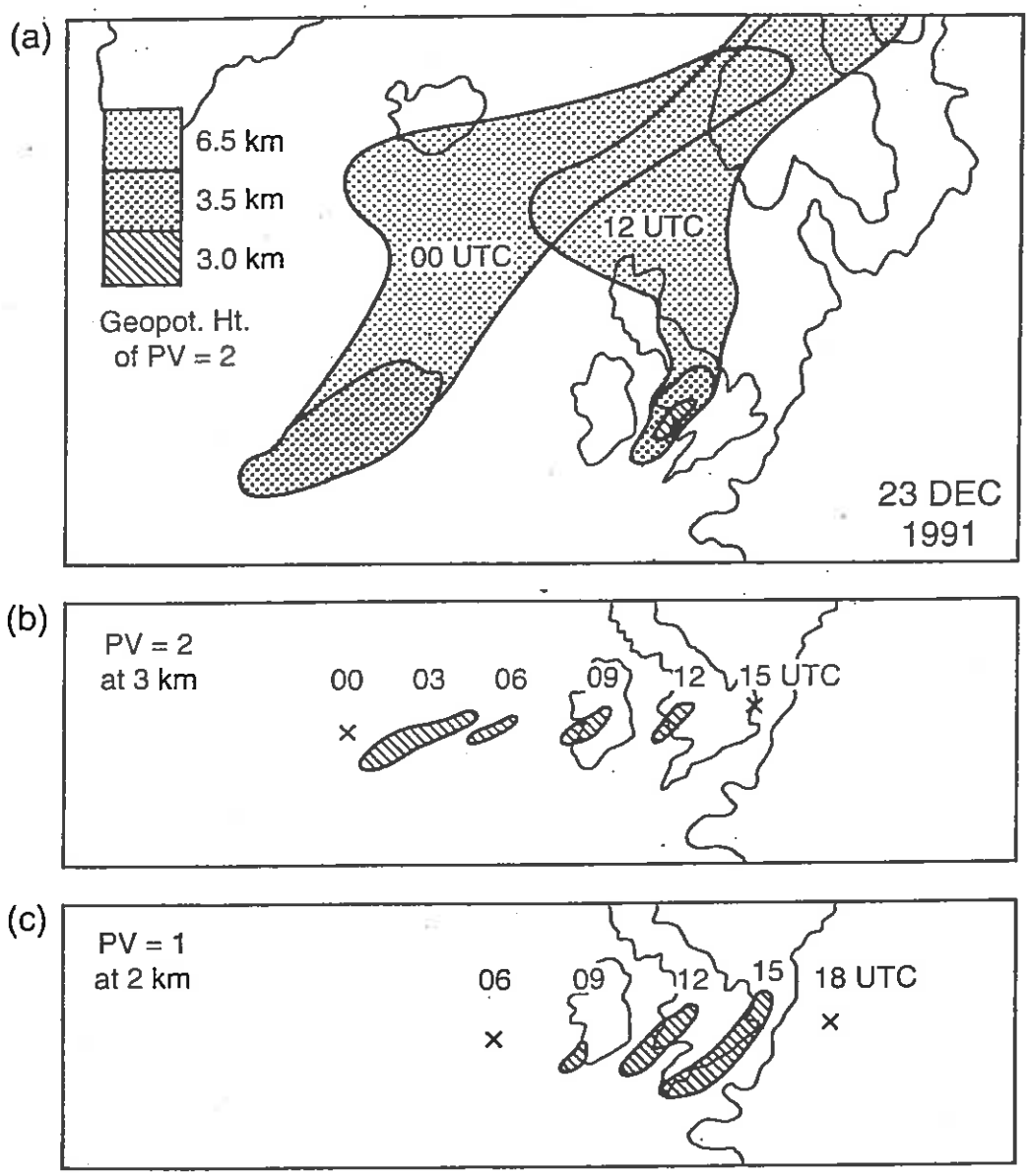
(a)
6.5 km
3.5 km
3.0 km
Geopot. Ht.
of PV = 2
00 UTC
12 UTC
23 DEC
1991
(b)
PV = 2
at 3 km
00
03
06
09
12
15 UTC
(c)
PV = 1
at 2 km
06
09
12
15
18 UTC

Fig 13

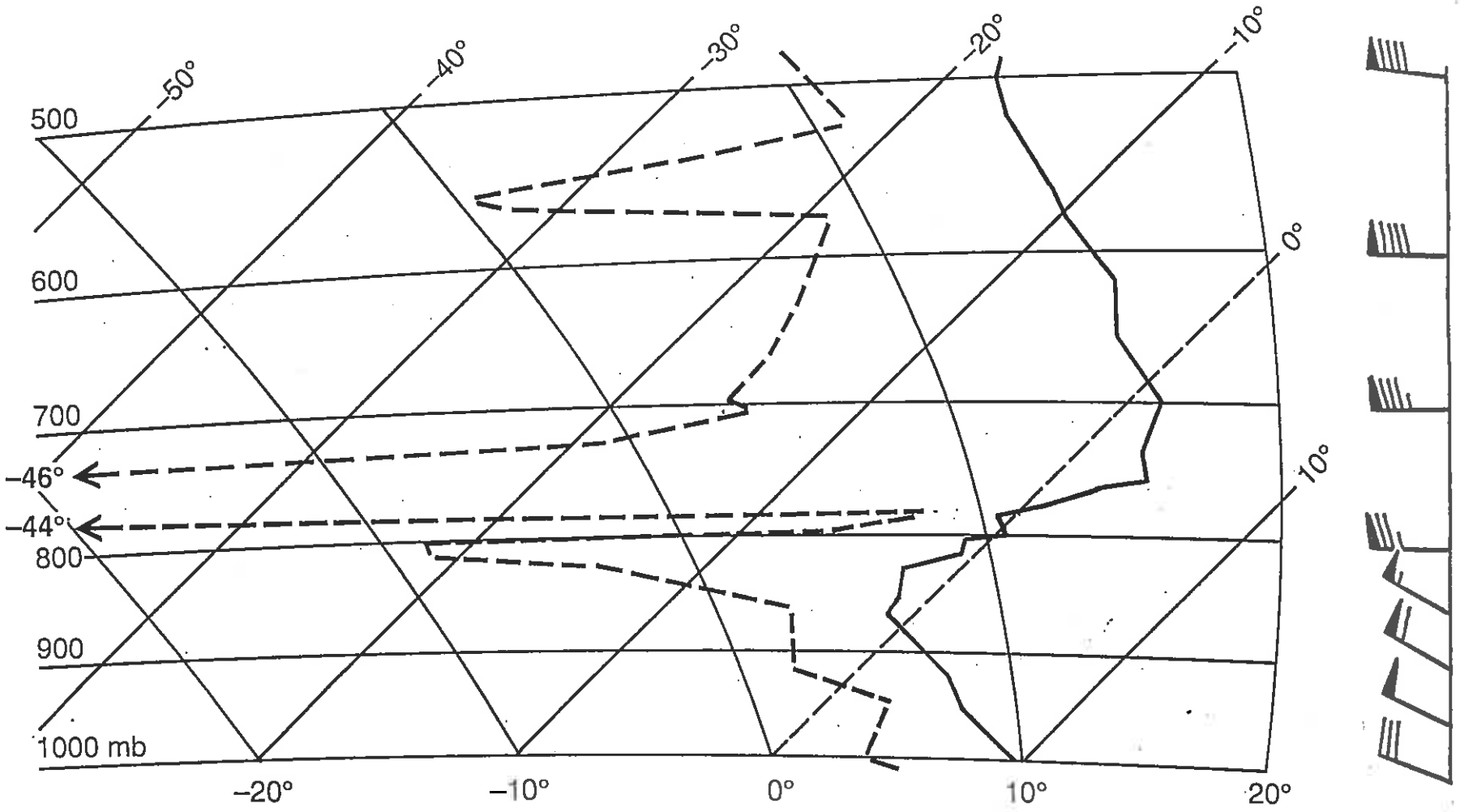

Fig 14

Fig 15

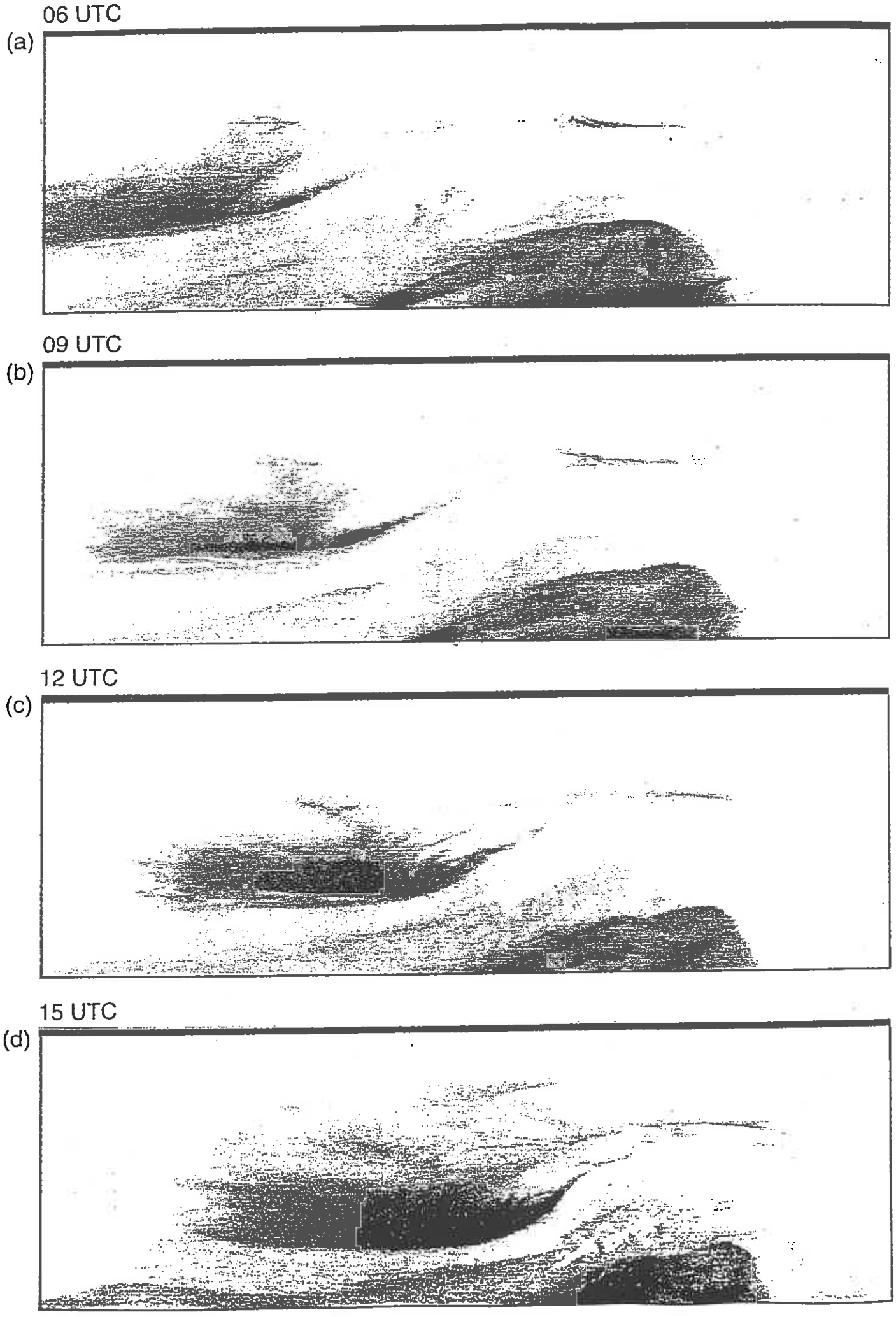

06, 09, 12, 15 UTC

(e)

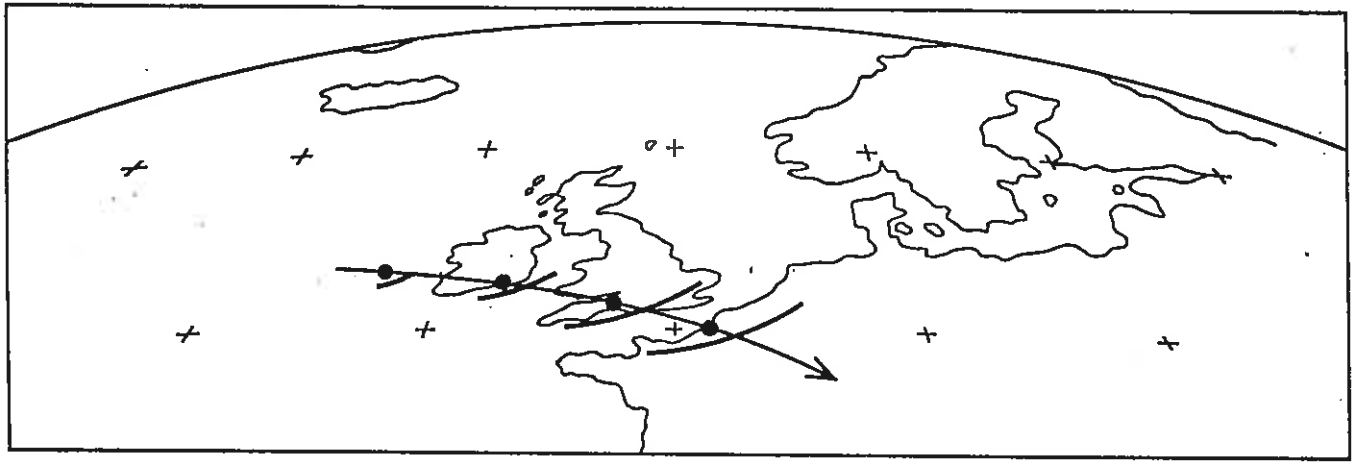

Fig 15(e)

CURRENT JCMM INTERNAL REPORTS

This series of JCMM Internal Reports, initiated in 1993, contains unpublished reports and also versions of articles submitted for publication. The complete set of Internal Reports is available from the National Meteorological Library on loan, if required.

1. **Research Strategy and Programme.**
   K A Browning et al
   January 1993

2. **The GEWEX Cloud System Study (GCSS).**
   GEWEX Cloud System Science Team
   January 1993

3. **Evolution of a mesoscale upper tropospheric vorticity maximum and comma cloud from a cloud-free two-dimensional potential vorticity anomaly.**
   K A Browning
   January 1993

4. **The Global Energy and Water Cycle**
   K A Browning
   July 1993

5. **Structure of a midlatitude cyclone before occlusion.**
   K A Browning and N Roberts
   July 1993

6. **Developments in Systems and Tools for Weather Forecasting.**
   K A Browning and G Szejwach
   July 1993

7. **Diagnostic study of a narrow cold frontal rainband and severe winds associated with a stratospheric intrusion.**
   K A Browning and R Reynolds
   August 1993

Met Office Joint Centre for Mesoscale Meteorology Department of Meteorology
University of Reading PO Box 243 Reading RG6 6BB United Kingdom
Tel: +44 (0)118 931 8425 Fax: +44 (0)118 931 8791
www.metoffice.com